Developmental Biology
Neuroscience

Microtubule networks in zebrafish hair cells facilitate presynapse transport and fusion during development

Reviewed Preprint
v1 • June 28, 2024
Not revised

Saman Hussain, Katherine Pinter, Mara Uhl, Hiu-Tung Wong, Katie Kindt

Section on Sensory Cell Development and Function, National Institute on Deafness and other Communication Disorders, Bethesda, MD, 20892, USA • Presynaptogenesis and Intracellular Transport in Hair Cells Junior Research Group, Institute for Auditory Neuroscience and InnerEarLab, University Medical Center Goettingen, 37075 Goettingen, Germany • Collaborative Research Center 889 'Cellular Mechanisms of Sensory Processing', 37075 Goettingen, Germany

Abstract

Sensory cells in the retina and inner ear rely on specialized ribbon synapses for neurotransmission. Disruption of these synapses is linked to visual and auditory dysfunction, but it is unclear how these unique synapses are formed. Ribbon synapses are defined by a presynaptic density called a ribbon. Using live-imaging approaches in zebrafish, we find that early in hair-cell development, many small ribbon precursors are present throughout the cell. Later in development, fewer and larger ribbons remain, and localize at the presynaptic active zone (AZ). Using tracking analyses, we show that ribbon precursors exhibit directed motion along an organized microtubule network towards the presynaptic AZ. In addition, we show that ribbon precursors can fuse together on microtubules to form larger ribbons. Using pharmacology, we find that microtubule disruption interferes with ribbon motion, fusion, and normal synapse formation. Overall, this work demonstrates a dynamic series of events that underlies formation of a critical synapse required for sensory function.

eLife assessment

This **important** study provides new insights into the maturation of ribbon synapses in zebrafish neuromast hair cells. **Convincing** evidence, based on live-cell imaging and pharmacological and genetic manipulations, is provided to show that the formation of this synaptic organelle is a dynamic process involving the fusion of presynaptic elements and microtubule transport. These findings will be of interest to neuroscientists studying synapse formation and function and should inspire further research into the molecular basis for synaptic ribbon maturation.

https://doi.org/10.7554/eLife.98119.1.sa3

Introduction

The inner ear and retina contain sensory cells that rely on specialized ribbon synapses that faithfully transmit the timing, duration, and intensity of sensory stimuli to the brain. Ribbon synapses are critical for human hearing and vision–disruption of these synapses is linked to auditory and visual disorders (Frederick and Zenisek, 2023; Kujawa and Liberman, 2015). The hallmark feature of these synapses is a presynaptic specialization called a ribbon, which is a dense body made up primarily of the protein Ribeye (Schmitz et al., 2000). Ribbons are found at the presynaptic active zone (AZ) and act as a scaffolds to ready synaptic vesicles for release (Schmitz, 2009). During development, small ribbon precursors are hypothesized to migrate to the presynaptic AZ and fuse to form larger, mature ribbons. However, there is no direct evidence for precursor migration or fusion, and the dynamic processes underlying ribbon formation remain unclear.

Neurotransmission at mature ribbon synapses is triggered in response to graded membrane depolarizations dictated by the duration and intensity of sensory stimuli. Membrane depolarization opens voltage-gated calcium channels (Ca_V1) beneath ribbons (Brandt et al., 2003; Chang et al., 2006) (see schematic in **Figure 1C**). Calcium influx triggers the fusion of synaptic vesicles secured near the ribbon, resulting in release of the glutamate onto postsynaptic receptors (Obholzer et al., 2008; Ruel et al., 2008). Studies in mouse and zebrafish have shown that Ribeye, along with $Ca_V1.4$ (photoreceptors) and $Ca_V1.3$ (hair cells) channels play important, interconnected roles in the formation of ribbon synapses (Jia et al., 2014; Mansergh et al., 2005; Nemzou N. et al., 2006; Sheets et al., 2012). For example, in mice and zebrafish lacking functional Ca_V1 channels, ribbon formation is disrupted, and fewer complete synapse are formed. Similarly, when Ribeye is knocked out in mouse or zebrafish, Ca_V1 channel localization is disrupted at ribbon synapses of photoreceptors and hair cells (Jean et al., 2018; Maxeiner et al., 2016; Sheets et al., 2011). In addition to Ribeye, the classic neuronal scaffolding proteins Bassoon and a novel variant of Piccolo, Piccolino have been shown to be important components of ribbon synapses (Gundelfinger et al., 2016). In mice, work has shown that in sensory cells lacking Bassoon ribbons are not properly anchored at the presynaptic AZ, and synapse function is disrupted (Dick et al., 2003; Frank et al., 2010; Khimich et al., 2005). In rats, loss of Piccolino also impacts ribbon morphology (Michanski et al., 2023; Regus-Leidig et al., 2014). Currently how these key molecular players fit within the dynamics underlying ribbon formation is not completely understood.

In neurons, precursor vesicles containing Piccolo and Bassoon have been shown to be transported along a network of microtubule tracks to the developing presynaptic AZ. (Ahmari et al., 2000; Gundelfinger et al., 2016; Maas et al., 2012; Shapira et al., 2003). Transport requires molecular motors, along with adaptor proteins, to move cargos along microtubules in a directional manner (Bury and Sabo, 2011; Fejtova et al., 2009; Maas et al., 2012). In neurons, kinesins are the molecular motors that transport cargos in the anterograde direction–away from the cell body and towards the presynaptic AZ, and cytoplasmic dynein is the motor that moves cargos in a retrograde manner (Sweeney and Holzbaur, 2018). Although it is currently unclear what kinesin transports Piccolo-Bassoon transport vesicles, recent work in *Drosophila* and *C. elegans* suggests that the kinesin KIF1A may transport AZ components (Oliver et al., 2022; Pack-Chung et al., 2007). Work in developing photoreceptors, has shown that ribbon precursors contain not only Ribeye, but also Bassoon, and the ribbon synapse specific isoform of Piccolo, Piccolino (Regus-Leidig et al., 2009). Further, work in developing mouse auditory inner hair cells (IHCs) has shown that ribbon precursors contain both Piccolino and Ribeye (Michanski et al., 2019). Whether these precursors are actively transported along microtubules during ribbon-synapse formation as in neurons is not known.

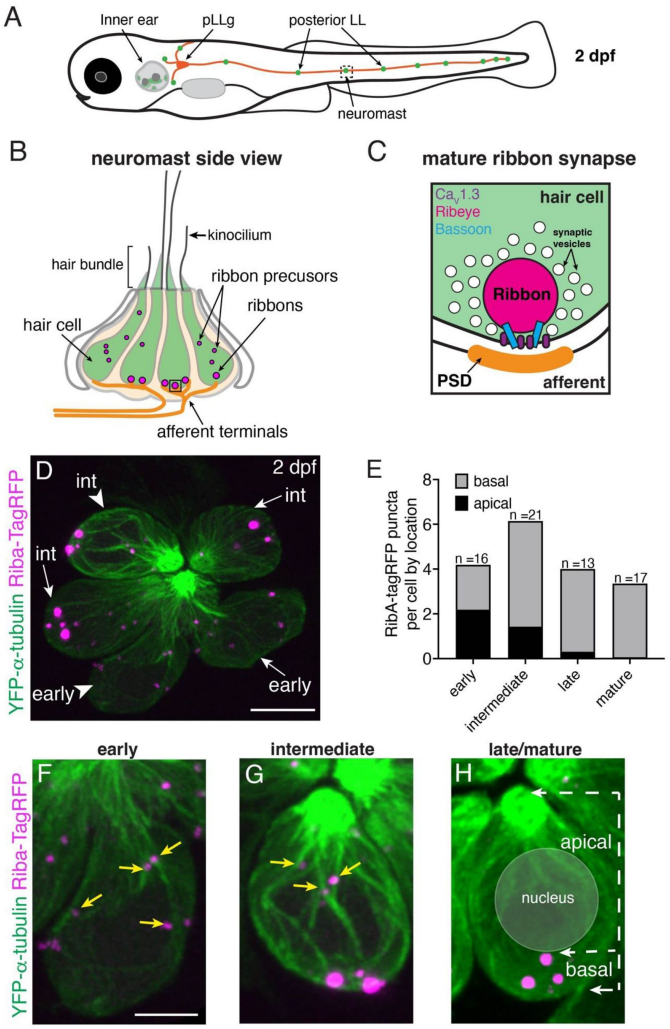

Figure 1

Ribbons associate with microtubules and change localization during development A)

Schematic of a larval zebrafish at 2 days post fertilization (dpf) with the location of the posterior-lateral line (LL) indicated relative to the zebrafish inner ear. Neuromasts (green) in the posterior LL contain sensory hair cells that are innervated by afferent projections from the posterior LL ganglion (pLLg, orange). **B)** Schematic of a neuromast at 2 dpf, viewed from the side. At 2 dpf, the majority of hair cells (green) are developing. A shorter kinocilium (part of the mechanosensory hair bundle) and an abundance of small ribbon precursors are indicative of an immature stage. **C)** Schematic of a ribbon synapse when mature. The dense presynapse or ribbon is made primarily of Ribeye. Ribbons tether synaptic vesicles near $Ca_V1.3$ channels at the plasma membrane, across from the postsynaptic density (PSD). Bassoon acts to anchor ribbons at the presynaptic AZ. **D)** Example image of a neuromast at 2 dpf, viewed from top down. The microtubule network and ribbons are marked with YFP-Tubulin and Riba-TagRFP respectively. In this example of 6 developing hair cells, 2 early and 4 intermediate cells are present. The cell bodies of an early and intermediate cell from this example (arrowheads) are expanded in **F** and **G**. **E)** Plot shows the average number of ribbons per hair cell at each developmental stage. Cell stage is determined by the height of the kinocilium. After an increase in ribbon number with development, there is a decrease upon maturation. The number of apically-localized Riba- TagRFP puncta is high at early and intermediate stages, and is lower in late and mature hair cells. In contrast, the number of basally-localized Riba-TagRFP puncta is low at early stages, and becomes higher by intermediate stages (n = 16, 21, 13, 17 hair cells for early, intermediate, late and mature stages respectively). **F-H)** Example images of hair cells expressing YFP-Tubulin and Riba-TagRFP at early, intermediate and late stages. At the early stage, Riba-TagRFP puncta are spread throughout the cell body and are smaller in size. At the intermediate stage, the number of Riba-TagRFP puncta become more basally enriched and appear larger in size. In late and mature hair cells, all Riba-TagRFP puncta are at the base of the cell and fewer in number. The arrows in **H** highlight the apical and basal region of the cell used for quantification of Riba- TagRFP puncta location in **E**. Scale bars in **D** = 5 μm and in **F** = 2 μm.

Ribbon-synapse formation has been well studied using light and electron microscopy in fixed tissues (Michanski et al., 2019; Regus-Leidig et al., 2009; Schmitz, 2009; Sheets et al., 2011; Sobkowicz et al., 1986, 1982). Studies in mouse auditory inner hair cells (IHCs) have shown that the majority of ribbon-synapse formation spans a large time window: E18-P14 (Michanski et al., 2019; Sobkowicz et al., 1986, 1982). In contrast to mice, ribbon synapses form along a condensed timeline in zebrafish hair cells: 12-18 hrs (Dow et al., 2015; Sheets et al., 2011). In both mouse IHCs and zebrafish hair cells, at the earliest stages of development there are many small ribbon precursors throughout the cell–these precursors are thought to form via self-aggregation of Ribeye within the cytosol (Magupalli et al., 2008; Schmitz et al., 2000). As development progresses ribbons become larger, localize to the presynaptic AZ and associate with the innervating afferent processes. Finally, the number of ribbons associated with postsynaptic machinery is refined to obtain the proper number of complete synapses. Recent work in mice has shown that ribbon precursors associate with microtubules (Michanski et al., 2019), and it has been proposed that ribbon precursors migrate along tracks of microtubules to reach the presynaptic AZ and during synapse refinement. Currently the *in vivo* dynamics of ribbon precursors and microtubules during these developmental events are not known.

To understand how ribbons form, we have studied hair cells and developing ribbons in the zebrafish lateral line (**Figure 1A**). The lateral line is a sensory system that allows aquatic vertebrates to sense local water movements (Freeman, 1928; Suli et al., 2012). This sensory system is composed of clusters of hair cells called neuromasts that are arranged in lines along the surface of the fish. The posterior lateral line (pLL) forms an array of neuromasts along the zebrafish trunk; in the pLL hair cells begin to form when larvae are 2 days post fertilization (dpf) (see **Figure 1A-B**, D). By 5 dpf, the majority of hair cells are mature, and the lateral-line system is functional (Suli et al., 2012). At these early ages zebrafish are transparent, and hair cells in the lateral line can easily be studied *in vivo* for durations encompassing large portions of ribbon formation (Dow et al., 2015). Further, transgenic lines expressing fluorescently tagged proteins allow the visualization of subcellular dynamics, such as ribbon formation, in living zebrafish, at high resolution.

During our study, we have worked in close collaboration with another group focused on later aspects of ribbon formation and refinement in mouse auditory IHCs (at postnatal stages). This work is published in a companion paper (Vorn et al.). Together our studies demonstrate that ribbon transport along microtubules networks is important to properly form ribbons during hair-cell development in mouse and zebrafish. Our *in vivo* zebrafish work leverages transgenic lines that label: developing ribbons, microtubule networks, and the growing plus-ends of microtubules. We use these lines, along with high-resolution imaging to visualize the dynamics of ribbon formation. Using live imaging, we show that at the earliest stages of synapse development, many small ribbon precursors are present throughout the cell. At later stages fewer, larger ribbons remain, and localize to the base of the cell. We find that microtubule networks in lateral-line hair cells are highly dynamic and grow plus-ends towards the presynaptic AZ (the direction taken by most kinesin motors) (Sweeney and Holzbaur, 2018). Using tracking analyses, we show that during development, ribbon precursors show directed motion towards the presynaptic AZ. Further, we show that ribbon precursors move along and can fuse together on microtubules. Lastly, we find that an unperturbed microtubule network is critical for ribbon motion, fusion, and normal ribbon-synapse formation. Overall, this foundational knowledge of ribbon formation provides fundamental insight on processes needed to reform ribbon synapses that are lost, such as after noise-induced and age-related hearing loss.

Results

Time-course of ribbon formation in living zebrafish lateral-line hair cells

Fixed preparations in zebrafish and mice have outlined a conserved process that underlies ribbon or presynapse development in hair cells (Michanski et al., 2019; Sheets et al., 2011). At the earliest stages of development, small ribbon precursors are found free-floating throughout the cytoplasm. When mature, ribbons are found predominantly at presynaptic AZs, opposing postsynaptic densities. To examine the dynamics underlying ribbon formation in more detail, we studied hair cells in the zebrafish pLL. These hair cells form 3-4 ribbon synapses in just 12-18 hrs (Dow et al., 2015; Kindt et al., 2012). To image hair cells, ribbon precursors and ribbons *in vivo* we used a double transgenic line. One transgenic line labels microtubules and serves as a hair-cell marker (*myo6b:YFP-tubulin*). The other transgenic line labels ribbons and smaller ribbon precursors (*myo6b:riba-TagRFP*) in hair cells (example, **Figure 1D**).

For our initial analyses, we assessed the overall time course of ribbon formation in hair cells in the posterior lateral-line (pLL) when larvae were 2 dpf (**Figure 1A**). At 2 dpf each neuromast contains 4-8 developing hair cells at different developmental stages (**Figure 1B,D**,F- H). We used the height of the kinocilium (see schematic in **Figure 1B**), the tallest part of the apical hair bundle (mechanosensory structure), to estimate the developmental stage of hair cells as described previously (Stage: hair bundle height; early: <1.5 µm, intermediate: 1.5-10 µm, late: 10-18 µm, mature: >18 µm (Zhang and Kindt, 2022)). Qualitatively, we observed that at early and intermediate stages, small Riba-TagRFP puncta were present throughout the cell body (examples, **Figure 1D,F**-G). By late stages, or in newly matured hair cells, larger Riba- TagRFP puncta were restricted to the base of the cell (example, **Figure 1H**). We quantified the total number of Riba-TagRFP puncta based on developmental stage and found that the total number of puncta was high at early and intermediate stages, but significantly decreased when hair cells were mature (**Figure 1E**, **Figure 1**-S1A, n = 7 neuromasts and 67 hair cells).

When taking these live images, we had no postsynaptic marker and were unable to differentiate between precursors and smaller ribbons associated with a postsynaptic density. Therefore, we classified all apical Riba-TagRFP puncta above the nucleus as precursors, and all ribbons located beneath the nucleus at the cell base were classified as more mature ribbons. Using this classification, we quantified the total number of Riba-TagRFP puncta at each developmental stage (Figure E, **Figure 1**-S1B-C, n = 7 neuromasts and 67 hair cells). We found that apical Riba-TagRFP precursors were only present at early and intermediate stages (**Figure 1E**, **Figure 1**-S1B, and see yellow arrows in **Figure 1F-G**). In contrast, hair cells at late stages or newly mature hair cells contained more mature ribbons located at the cell base, below the nucleus (**Figure 1E,H**, **Figure 1**-S1C). Overall, our live images examining Riba-TagRFP puncta follows a similar, developmental process as observed in fixed preparations–the number of ribbons and precursors decrease and become basally localized to the presynaptic AZ as the hair cell develops.

Microtubule grow plus-ends toward the presynaptic active zone in hair cells

An important question in ribbon formation is how ribbons and precursors migrate to the presynaptic AZ. Work on mouse IHCs using electron microscopy (EM) and super-resolution microscopy found that developing ribbons and precursors often associate with microtubules (Michanski et al., 2019). Similar to what was observed in mice using EM, in living, lateral-line hair cells we observed ribbon precursors associate with microtubules (see yellow arrows in **Figure 1F-G**). Based on these association studies, a microtubule network may function to transport

ribbon precursors during development. To understand if ribbons could be transported along microtubules, we first examined the composition and polarity of the microtubule network in lateral-line hair cells.

We first examined the composition, or posttranslational modifications present in the microtubule network in lateral-line hair cells using immunohistochemistry. Using this approach, we labeled either acetylated- (modification found in mechanically stabilized microtubules) or tyrosinated- (modification found in destabilized microtubules) α-tubulin (Janke and Magiera, 2020). We performed our staining in a transgenic line that labels all microtubules (*myo6b:YFP- tubulin*). We found that in lateral-line hair cells, the microtubule network extends along the apico-basal axis of the cell and is highly acetylated; acetylated microtubules are more concentrated at the cell apex (**Figure 2**-S1A-C). Outside of the kinocilium, we did not observe a considerable amount of tyrosinated microtubules in lateral-line hair cells. Instead, tyrosinated microtubules were observed in the zebrafish skin, lateral-line nerve terminals and the supporting cells that surround hair cells (**Figure 2**-S1D-F). Overall, our immunostaining results indicates that in zebrafish lateral-line hair cells, a considerable portion of the microtubule network is highly acetylated. Acetylation could provide a population of mechanically stable microtubules that could be used to transport ribbon precursors.

Although microtubule modifications are informative, these labels do not provide definitive information regarding microtubule growth or polarity. Knowing microtubule polarity is important, as many cargos are transported based on polarity. For example, most kinesin motor proteins transport cargos toward the more dynamic plus-end of microtubules (Sweeney and Holzbaur, 2018). Therefore, to explore microtubule polarity in lateral-line hair cells, we created a transgenic line that expresses the plus-end marker of microtubules, EB3 (end-binding protein 3), fused with GFP (example, **Figure 2A**; *myo6b:EB3-GFP*). Previous work in other cell types has shown that EB3-GFP can be used to visualize the plus-end of growing microtubules (Kawano et al., 2022; Stepanova et al., 2003).

We used this transgenic line, along with confocal microscopy to visualize microtubule growth in lateral-line hair cells (z-stacks every 7 s for 20-30 minutes). By imaging EB3-GFP dynamics, we observed comet-like tracks that allowed us to visualize the plus-end of growing microtubules (see Movie S1). In hair cells, microtubule organizing centers are located beneath a single microtubule-based kinocilium, the primary cilium in hair cells (Lepelletier et al., 2013).

Consistent with studies in motile cilia, we observed a foci of EB3-GFP at the tips of kinocilia that emanate away from the apex of the cell body (Schrøder et al., 2011) (**Figure 2**-S2A-C). This result suggests that similar to other cilia, the plus ends of kinocilia are towards their tips, away from the cell body. In addition, we observed EB3-GFP tracks within hair-cell bodies and found that the majority of tracks were directed away from the cell apex and towards the base of the cell (see examples of EB3-GFP timelapse, with tracks rendered into a pseudocolor image based on time; **Figure 2C-D**). To quantify the direction of EB3-GFP tracks we used Imaris to perform 3D analyses to detect and create vectors of EB3-GFP tracks (see arrows; **Figure 2B,E**,F). We aligned these vectors along the apico-basal axis of each cell. Here vector movement towards the apex was represented as 180°, and movement to the base was represented at 0° (see schematic, **Figure 2G**). Movement of EB3-GFP vectors was quantified as the angle between 0 and 180°.

From this analysis we found that 77 % of EB3-GFP vectors were directed towards the base in lateral-line hair cells (2006/2598 tracks < 90°, n = 7 neuromasts and 33 hair cells,).

Overall, our immunostaining revealed that the soma of hair cells contains a population of microtubules stabilized by acetylation. Our *in vivo* imaging of EB3-GFP revealed that within this population there is extensive microtubules dynamics, and the plus ends of microtubules are primarily directed towards the cell base, and the presynaptic AZ.

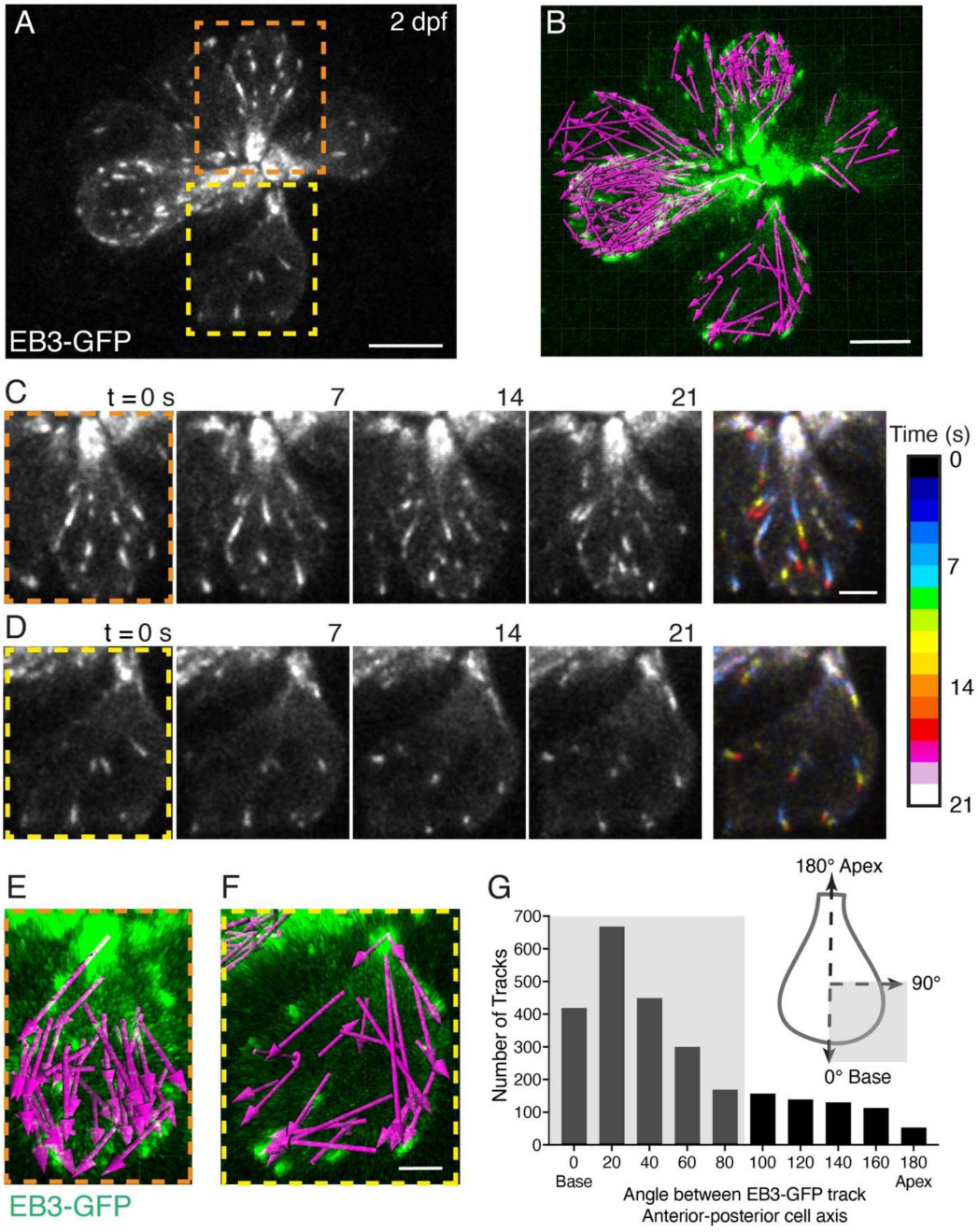

3

Figure 2

EB3-GFP tracks show plus-ends of microtubules move to the cell base **A)** Example image of a neuromast at 2 dpf. The growing or plus-ends of microtubules are marked with EB3-GFP. In this example the apex of 8 developing cells is at the center of the image and the base of each cell is at the periphery. 2 example cells are outlined (dashed lines) and expanded in more detail in **C-D,** and **E-F**. **B)** A 22 min timelapse was taken of the example in **A**. All EB3-tracks, indicated by magenta arrows (Tracked in Imaris) acquired during the timelapse are shown. **C-D)** Example time courses of EB3-GFP in hair cells over 21 s; the cell apex is towards the top of each image. In the final image, the 4 images for each example (0-21 s) were projected overtime as a pseudocolor image represented by the colormap. The pseudocolor images show that many EB3-GFP tracks move to the cell base. **E-F)** The magenta arrows in **E** and **F** show all the EB3-GFP tracks acquired in the example cells in **C-D** over the entire 22 min duration. Arrowheads indicate direction of travel. **G)** The schematic in **G** shows how EB3-GFP tracks were aligned to each hair cell. Tracks moving toward the apex have a track angle of 180°, while those moving to the base have an angle of 0°. This analysis revealed that the majority of EB3-GFP tracks (shaded domains) move toward the base of the cell (n = 7 neuromasts, 2597 tracks). Scale bars in **A** = 5 μm and in **C-F** = 2 μm.

Ribbon precursors associate with and show directed motion along microtubules

Our analysis of microtubule dynamics using EB3-GFP indicates that the plus ends of microtubules point towards the hair-cell base (**Figure 2**). Therefore, we hypothesized that these tracks of microtubules could be used by kinesin motor proteins to transport precursors from the cell apex to base during development. To test this hypothesis, we used either Airyscan or Airyscan 2 confocal imaging to capture timelapses of ribbon and precursor movement for longer durations (Airyscan: ~3 µm z-stacks (16-18 slices) every 50-100 s for 30-70 minutes) or for shorter total durations with a faster capture rate (Airyscan 2: ~2-3.5 µm z-stacks (12-20 slices) every 20 s for 15-45 minutes). We focused our analysis on developing lateral-line hair cells at early and intermediate stages when ribbon precursors are abundant throughout the cell (**Figure 1D,F**-G). For this work we used Riba-TagRFP to mark ribbons and precursors, and YFP- tubulin to label microtubules and provide cellular context. From our timelapses, we observed that similar to our initial live analyses (**Figure 1F-G**), many ribbon precursors associated with microtubules (Movie S2, S3). We also observed that precursors exhibited 3 main movement behaviors related to microtubule association. First, we observed that many precursors associated with microtubules remained stationary or confined (examples: **Figure 3C** top two panels, **Figure 3D,E** asterisks, Movie S4). Second, we also observed rapid movement of precursors–during this movement precursors appeared to be in close association with microtubules (examples: **Figure 3C** bottom 4 panels, **Figure 3D,E** yellow arrowhead, **Figure 3**- S1A,B Movie S4, S5). This movement along microtubules occurred bidirectionally, towards the cell apex and towards the base (**Figure 3C**, middle panels (arrows to base), bottom panels (arrows to apex); Movie S4 (to base), Movie S5 (to apex), **Figure 3**-S1A-B). Third, we often observed that precursors switched association between neighboring microtubules (**Figure 3**- S1C, Movie S6).

To quantify ribbon and precursor movement, we used Imaris to obtain x,y,z co-ordinates for each ribbon during our timelapses (Longer 30-70 minute acquisitions) (example, **Figure 3A**- C, Movie S2, S3). This analysis yielded tracks or trajectories for all precursors and ribbons. We then performed a mean-squared displacement (MSD) analysis on ribbon tracks to classify the type of motion we observed. In this analysis, the exponent (α) of MSD vs. time is obtained by curve fitting. A value of $\alpha > 1$ indicates directional motion with velocity, $\alpha = 1$ indicates Brownian motion and $\alpha < 1$ is representative of confined motion or subdiffusion (**Figure 3F,G**) (Sikora et al., 2017). This method allows us to determine what type of motion each track is exhibiting. Our results show that in developing hair cells, ribbon tracks exhibit directional as well as confined motion (**Figure 3H**, example MSD tracks with $\alpha < 1$ (red tracks, top panel) and $\alpha > 1$ (black tracks, bottom panel) from 2 neuromasts). Upon quantification, 19.2 % of ribbon tracks show $\alpha > 1$, indicative of directional motion (n = 7 neuromasts, 30 hair cells and 99 tracks). Overall, the vast majority (80.8 %) of ribbon tracks had $\alpha < 1$, indicative of confined motion. Of the tracks that showed directional motion, while the majority move to the cell base, we found that 21.2 % of ribbon tracks moved apically. This apical movement is consistent with a subpopulation of microtubules shows plus-end mediated growth apically (22.8 % of EB3-GFP tracks). Overall, our timelapse imaging demonstrated that ribbons and precursors displayed 3 main types of movement on microtubules: confinement, movement along microtubules and switching between microtubules. Further, our MSD analysis indicates that while the majority of precursors exhibit confined motion, a subpopulation of ribbons and precursors exhibit directional motion.

Long-term manipulation of microtubules impacts ribbon formation

Our timelapse imaging revealed that precursors and ribbons can move along microtubules in a directional manner. To assess the importance of the microtubule network in ribbon-synapse formation we used pharmacology to destabilize or stabilize the microtubule network in lateral-

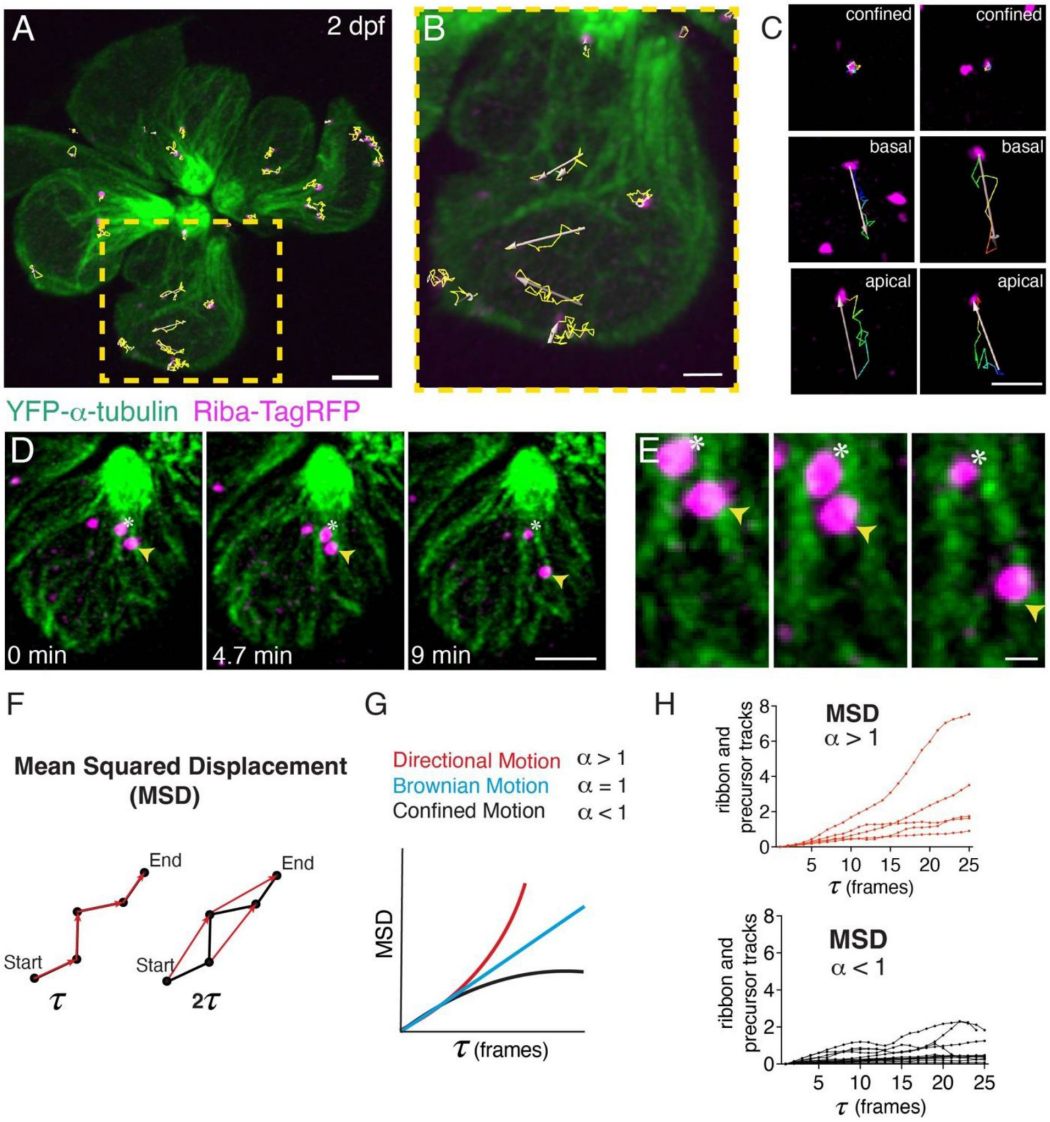

Figure 3

Ribbon precursors exhibit directional motion and confinement on microtubules **A-B)** To quantify motion, ribbons and ribbon precursors were tracked in early and intermediate stage hair cells at 2 dpf (example). Shown are tracks (in yellow) from an entire neuromast (**A**) and a single hair cell (**B**), obtained using in Imaris, during a 30 min timelapse acquired every 50 s (also see Movie S2). **C)** Magnified view showing individual tracks overtime show examples of confinement, and motion towards the cell base and apex. **D)** Example of confined motion and directed motion on microtubules in a single hair cell. Movie was obtained during a 9 min timelapse acquired every 20 s. The ribbon labeled by the asterisks remains confined, while the ribbon labeled with the yellow arrow moves along a microtubule, towards the cell base, over time. **E)** A magnified image of the example shown in **D. F)** Mean squared displacement (MSD) vs time was used to measure movement behaviors. The results are plotted in the form of MSD vs time step (τ) plots and the exponent (α) of the plots can be used to distinguish between the different types of motion observed (confined, directional or Brownian motion). Tracks that move directionally with a velocity have α > 1, where α is the exponent of the MSD vs time curve. MSD can also reveal tracks exhibiting confined diffusion (α < 1), i.e., bound to the microtubule but not moving. **H)** Example MSD plots of individual ribbon tracks from 2 control neuromasts (15 tracks MSD <1, 5 tracks MSD>1). The tracks that move directionally with a velocity have α > 1 are in red, while tracks that are confined with a velocity α < 1 are in black. Scale bar in **A** = 2 μm, **B-D** = 1 μm and in **E** = 500 nm.

line hair cells using nocodazole or taxol respectively. We verified the effectiveness of our pharmacological treatments by imaging microtubule dynamics in lateral-line hair cells (*myo6b:YFP-tubulin*). We used Airyscan confocal microscopy to acquire timelapses of YFP- tubulin after a 30-min pharmacological treatment (3 µm z-stacks, every 50-100 s for 30-70 min). These timelapses revealed that compared to controls, 250-500 nM nocodazole and 25 µM taxol dramatically destabilized and stabilized microtubules in lateral-line hair cells (examples see Movie S7). After verifying the effectiveness of our pharmacological treatments, we incubated larvae at 2 dpf for 16 hrs (56-72 hours post fertilization (hpf)), a time window that encompasses a large portion of ribbon-synapse formation in developing hair cells. After these pharmacological treatments we fixed and immunostained larvae to label acetylated-α-tubulin, to monitor changes to the microtubule network. In addition, we co-labeled with Ribeyeb to label ribbons and precursors and pan-Maguk to label postsynapses.

After a 16-hr treatment with 250 nM nocodazole we qualitatively observed a decrease in acetylated-α-tubulin label (examples, **Figure 4A,C**). Less acetylated-α-tubulin label indicates that our nocodazole treatment successfully destabilized microtubules. We also examined the number of hair cells per neuromast and observed that after nocodazole treatment, there were significantly fewer hair cells compared to controls. This indicates that either nocodazole is slightly toxic or it interferes with cell division. Both situations have been observed previously during nocodazole treatments in other systems (Gupta, 1985; Zieve et al., 1980). We next examined the Ribeyeb label in hair cells to assess precursors and ribbons. We observed that the average area of Ribeyeb puncta was significantly reduced compared to controls (**Figure 4H**). Further, the relative frequency of Ribeyeb puncta with smaller areas was higher in nocodazole treated hair cells compared to controls (**Figure 4I**). We used cutoff of 0.1 μm^2 to estimate the number of precursors among the Ribeyeb puncta (**Figure 4I**, > 0.1 μm^2, gray shaded bar encompasses the precursor population). Using this cutoff to identify precursors, we found that there were significantly more precursors per hair cell in nocodazole treatment compared to controls (**Figure 4G**). We also examined the number of complete synapses (Ribeyeb-Maguk paired puncta) per hair cell after nocodazole treatment. We found that there were significantly fewer complete synapses per hair cell after a 16-hr nocodazole treatment (**Figure 4F**). Overall, our long-term nocodazole treatment indicated that microtubule destabilization resulted in more ribbons precursors and the formation of fewer synapses per cell.

We performed a similar analysis on hair cells after a 16-hr treatment with 25 µM taxol. Qualitatively more acetylated-α-tubulin label was observed after treatment, indicating that our taxol treatment successfully stabilized microtubules (examples, **Figure 4**-S1A,C). Unlike nocodazole treatment, taxol did not significantly impact the number of hair cells, the average area of Ribeyeb puncta or number of precursors per hair cell compared to controls (**Figure 4**- S1E,G-H). Interestingly, we observed slightly more complete synapses per hair cell after a 16-hr taxol treatment (**Figure 4**-S1F). Overall, our long-term taxol treatment indicated that microtubule stabilization did not dramatically impact synapse formation in lateral-line hair cells.

Together this pharmacology study revealed that long-term destabilization and stabilization of microtubules during development can impact ribbon formation in lateral-line hair cells. Microtubule destabilization had the most dramatic effect leading to more ribbon precursors and the formation of fewer complete synapses.

Kif1aa mutants have fewer synapses and more ribbon precursors

In order for cargo (such as ribbons and precursors) to be transported along microtubules, molecular motor proteins are required. Kinesin motor proteins transport cargos along microtubules towards the growing, plus end. Our work demonstrated that in hair cells of the lateral line, the plus-end of microtubules grow from the apex to base of the cell (**Figure 2**).

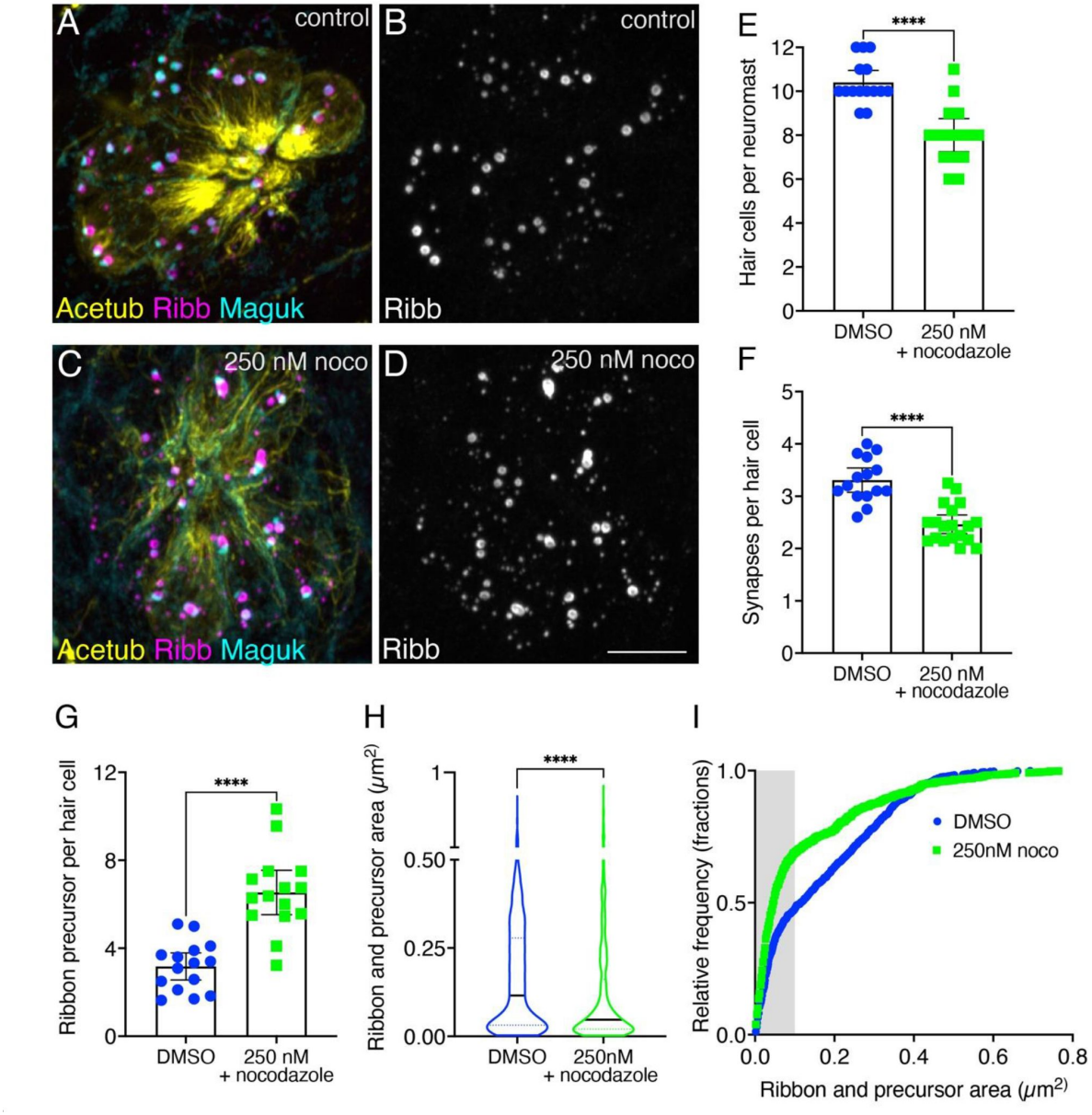

Figure 4

Overnight microtubule destabilization increases precursor numbers and decreases synapse counts **A-D)** Example immunostain of a neuromasts at 3 dpf after an overnight treatment with 250 nM nocodazole (**C-D**) or DMSO (**A-B**). Acetylated α-tubulin (Acetub) labels microtubules, Ribeyeb (Ribb) labels precursors and ribbons, and Maguk labels postsynapses. **E-G**) After an overnight treatment with 250 nM nocodazole there are significantly fewer hair cells per neuromast (**E**, $P < 0.0001$), fewer complete synapses per cell (**F**, $P < 0.0001$), and more ribbon precursors per cell (**G**, $P < 0.0001$) compared to controls (n = 15 neuromasts for control and 250 nM nocodazole treatments). **H-I**) After an overnight treatment with 250 nM nocodazole the average area of Ribeyeb puncta was significantly lower compared to controls (**H**, $P < 0.0001$, n = 1008 and 1135 Ribeyeb puncta for control and 250 nM nocodazole treatments). In **I**, the relative frequency of all the areas of Ribeyeb puncta are plotted in nocodazole treatment and controls. The shaded area in **I** shows the areas (areas < 0.1 μm^2) used to quantify precursor numbers in **G**. For comparisons an unpaired t-test was used in **E-G**, and a Mann-Whitney test was used in **H**. Scale bar in **D** = 5 μm.

Single cell RNA sequencing (scRNAseq) has revealed that *kif1aa*, a zebrafish orthologue of Kif1a, a plus-end directed kinesin motor protein, is highly expressed in lateral-line hair cells (Lush et al., 2019). In zebrafish there are 2 orthologues of mammalian *Kif1a*, *kif1aa* and *kif1ab*. While scRNAseq in zebrafish has shown that *kif1ab* and *kif1aa* are widely co-expressed in the nervous system, lateral-line hair cells express just *kif1aa* (Lush et al., 2019; Sur et al., 2023). Therefore, we tested whether Kif1aa could be the kinesin motor that transports ribbons and precursors to the cell base during development.

To test for a role of Kif1aa in zebrafish hair cells, we created a CRISPR-Cas9 mutant (Varshney et al., 2016). Our *kif1aa* mutant has a stop codon in the motor domain and is predicted to be a null mutation (**Figure 5**-S1A-B). For our initial analysis, we co-labeled hair cells at 3 dpf with Ribeyeb to label ribbons and precursors and pan-Maguk to label postsynapses (see examples **Figure 5A-D**). This is a similar end point used to examine synapse formation after our long-term nocodazole and taxol treatments (**Figure 4** and **Figure 4**-S1). We found that at 3 dpf *kif1aa* mutants had a similar number of hair cells per neuromast (**Figure 5E**). Despite a similar number of hair cells, we found that there were significantly fewer complete synapses per hair cell in *kif1aa* mutants compared to controls (**Figure 5F**). In addition, we found that there were significantly more ribbon precursors in *kif1aa* mutants compared to controls (**Figure 5G,H**,I). As described in the previous section, we also observed fewer complete synapses and more ribbon precursors after a 16-hr nocodazole treatment (**Figure 4F,G**). Together, this suggests that both intact microtubules and Kif1aa are required for normal ribbon-synapse formation.

Short-term disruption of microtubules, but not loss of Kif1aa, impacts ribbon formation

Our initial experiments suggest that microtubule networks and Kif1aa are important for proper ribbon-synapse formation in lateral-line hair cells. But the actual changes in precursors and ribbons within developing hair cells was unclear. Therefore, we examined changes in ribbons and precursors in living lateral-line hair cells over 3-4 hrs of development. For our analysis we used transgenic lines expressing YFP-tubulin to monitor microtubules and Riba-TagRFP to monitor precursors and ribbons *in vivo*. We examined precursors and ribbons after nocodazole or taxol treatment, or after knockdown of Kif1aa during this developmental window.

For our pharmacology experiments we first acquired Airyscan confocal images of developing hair cells at 2 dpf that express YFP-tubulin and Riba-TagRFP. Then after a 3-4 hr treatment in either 500 nM nocodazole or 25 μM taxol we reimaged the same hair cells.

Consistent with our previous results (**Figure 4** and **Figure 4**-S1) nocodazole and taxol treatments qualitatively destabilized or stabilized microtubules respectively (**Figure 6A-F**). In each developing cell, we quantified the number of Riba-TagRFP puncta before and after each treatment. In our control samples we observed on average no change in the number of Riba-TagRFP puncta per cell (**Figure 6G**). Importantly we observed that nocodazole treatment led to a significant increase in the number of Riba-TagRFP puncta over time (**Figure 6G**). In contrast, similar to controls, taxol treatment did not alter the number of Riba-TagRFP puncta over time (**Figure 6G**).

Next, we used a similar approach to examine the number of Riba-TagRFP puncta in *kif1aa* mutants over a 3-4 hr time window. For this analysis, we examined puncta in *kif1aa* F0 crispants. These mutants are derived from injection of 2 *kif1aa* guide RNAs (gRNAs) and Cas9 protein. This approach has shown to be an extremely effective way to assay gene function in any genetic background (Hoshijima et al., 2019). Using this approach, we were able to robustly disrupt the *kif1aa* locus. We found that compared to uninjected controls, in *kif1aa* F0 crispants there was no

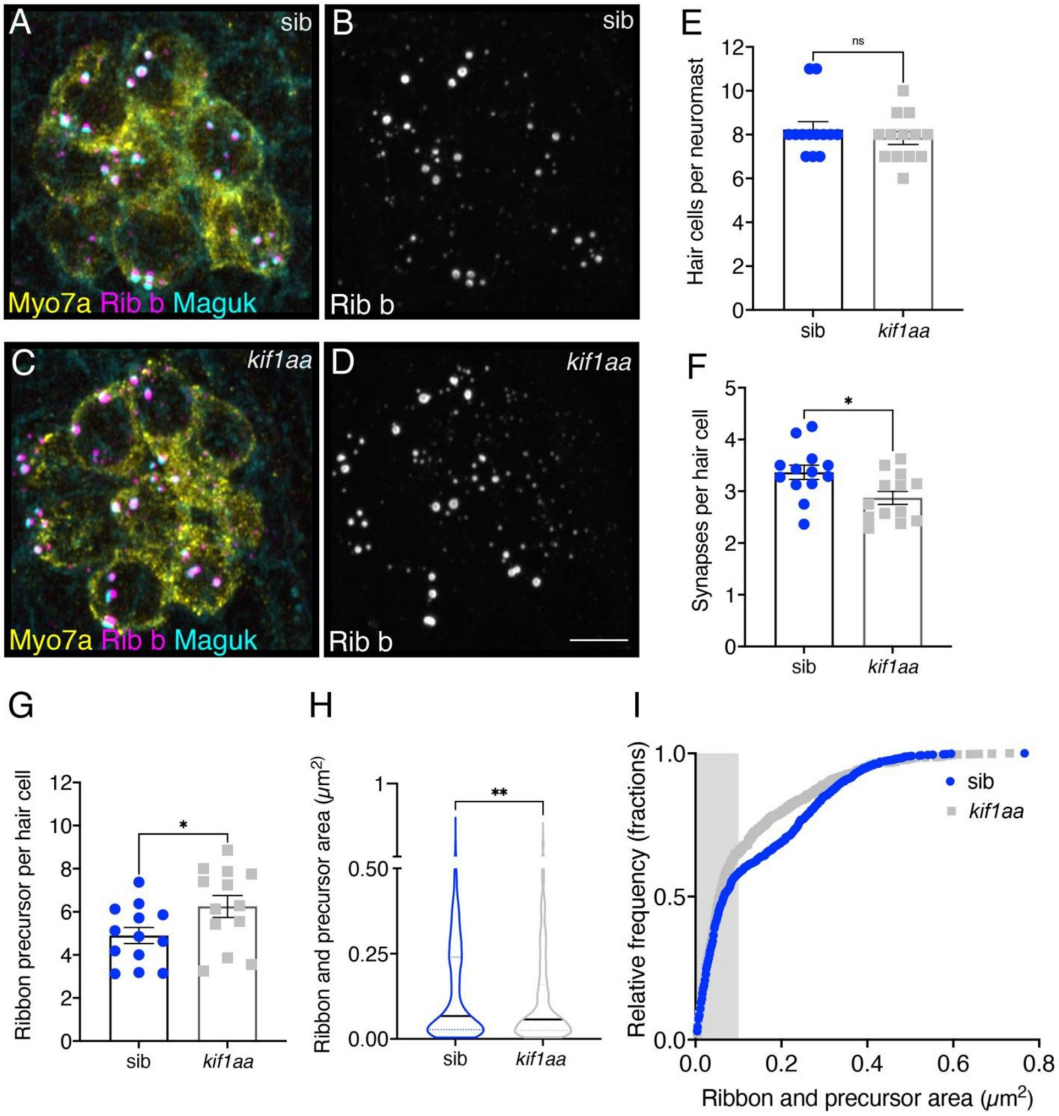

Figure 5

Loss of Kif1aa increases precursor numbers and decreases synapse counts **A-D)** Example immunostain of neuromasts at 3 dpf after in *kif1aa* germline mutants (**C-D**) or sibling control (**A-B**). Myosin7a labels hair cells, Ribeyeb (Ribb) labels precursors and ribbons, and Maguk labels postsynapses. **E-G**) In *kif1aa* mutants there is no change in the number of hair cells per neuromast (**E**, P = 0.418), but there are fewer complete synapses per cell (**F**, P = 0.014), and more ribbon precursors per cell (**G**, P = 0.044) compared to sibling controls (n = 13 neuromasts for control and *kif1aa* mutants). **H-I**) In *kif1aa* germline mutants the average area of Ribeyeb puncta was significantly lower compared to sibling controls (**H**, P = 0.005, n = 896 and 1008 Ribeyeb puncta for control and *kif1aa* mutants). In **I**, the relative frequency of all the areas of Ribeyeb puncta are plotted in *kif1aa* mutants and sibling controls. The shaded area in **I** shows the areas (areas < 0.1 μm^2) used to quantify precursor numbers in **G**. For comparisons an unpaired t-test was used in **E-G**, and a Mann-Whitney test was used in **H**. Scale bar in **D** = 5 μm.

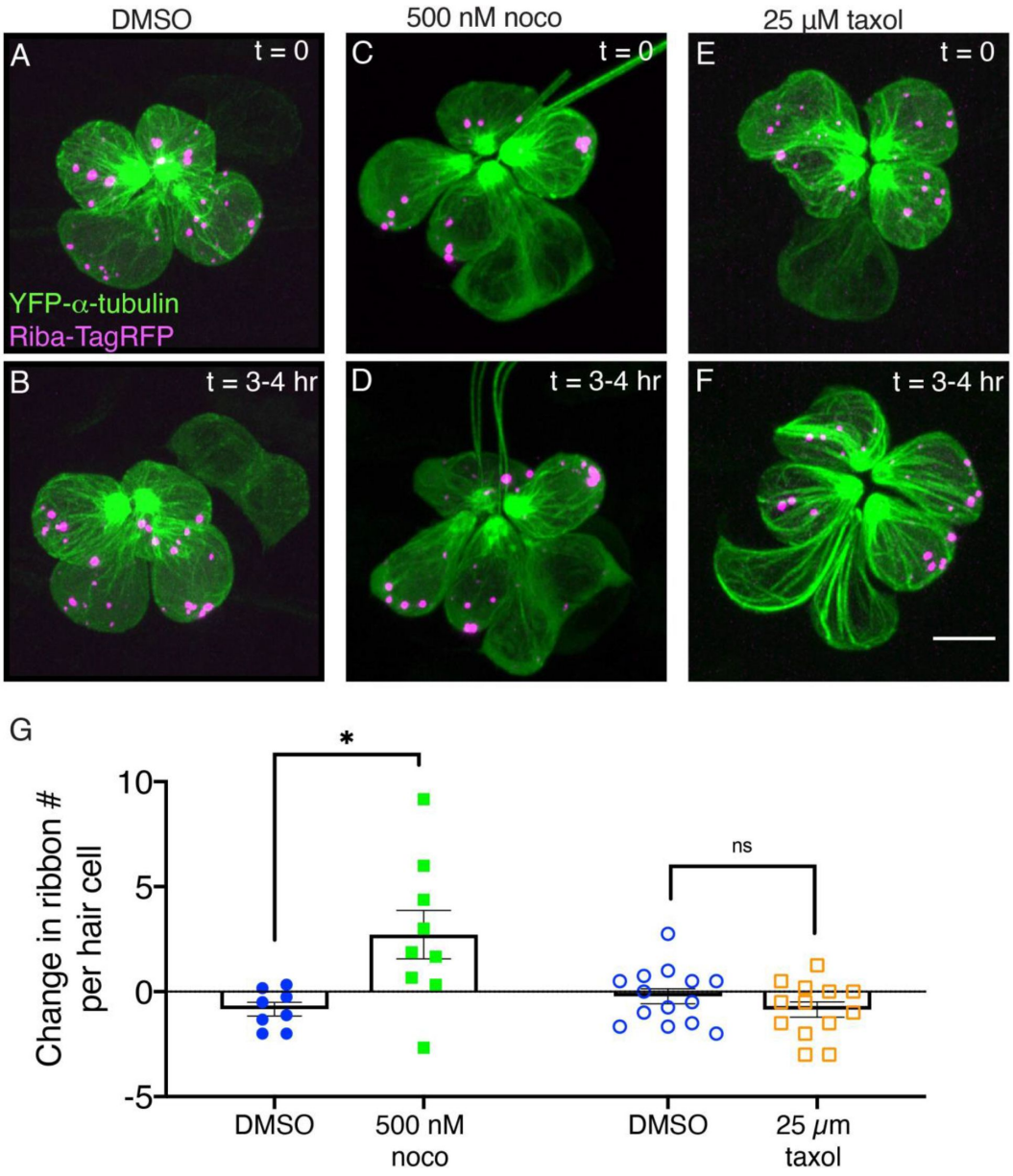

Figure 6

Microtubule destabilization increases ribbon numbers *in vivo* **A,C,E)** Example images of neuromasts at 2 dpf. The microtubule network and ribbons are marked with YFP-tubulin and Riba-TagRFP respectively. Neuromasts were imaged immediately after a 30-min treatment with DMSO (**A**, Control) 500 nM nocodazole (**C**) or 25 µM taxol (**E**), (t = 0). **B,D,F**) The same neuromasts in **A,C,E** imaged 3-4 hrs after treatment. **G**) Quantification revealed that after 3-4 hr nocodazole treatment, there were more Riba-TagRFP puncta per hair cell compared to controls (n = 9 and 8 neuromasts for nocodazole and DMSO, p = 0.013). In contrast after a 3-4 hr taxol treatment there was no significant change in the number of Riba- TagRFP puncta per hair cell compared to controls (n = 13 and 14 neuromasts for taxol and DMSO, p = 0.256). An unpaired t-test was used for comparisons in **G**. Scale bar in **F** = 5 µm.

change in the number of Riba-TagRFP puncta per cell over 3-4 hrs (**Figure 6**-S1A- F). Overall, live imaging over 3-4 hr time windows indicates that a loss of microtubule stability, but not loss of Kif1aa, results in an increase in Riba-TagRFP puncta within developing lateral-line hair cells.

Ribbons and precursors require microtubules, but not Kif1aa for directed motion

Our tracking analyses revealed that ribbons and precursors show directed motion on microtubules. Based on these results, we asked what happens to this movement if we disrupt microtubules or the kinesin motor Kif1aa. To test whether microtubules are required for directional ribbon and precursor motion, we used the drugs nocodazole and taxol to alter microtubule dynamics. We treated the fish with these drugs for 30 min and recorded timelapses of ribbon and precursor motion. This short treatment allowed us to observe ribbon motion relatively soon after microtubule disruption and minimize any cytotoxic effects of the compounds. Then we performed MSD analysis on the ribbon tracks to determine if directional motion was impaired (**Figure 7A**). We found that after destabilizing microtubules by treatment with 500 nM nocodazole for 30 minutes, the proportion of tracks with $\alpha > 1$ was significantly reduced compared to controls (**Figure 7C**). We also found that the proportion of longer tracks with a cumulative displacement > 1 µm was also reduced after nocodazole treatment compared to controls (**Figure 7B,F**). This analysis indicates that an intact microtubule network is needed for proper directional ribbon motion and longer displacements. In contrast, after stabilizing microtubules by treatment with 25 µM taxol, we observed no effect on the proportion of tracks with displacement > 1 µm or the proportion of tracks with $\alpha > 1$, compared to controls (**Figure 7D,G**).

Next, we used a similar approach to examine the tracks of ribbon and precursor motion in *kif1aa* mutants. For this analysis, we examined ribbon puncta in *kif1aa* F0 crispants. We observed that the proportion of tracks with displacement > 1 µm was not significantly different between *kif1aa* F0 crispants and controls (**Figure 7H**). Similarly, the proportion of tracks with $\alpha > 1$, was also not significantly different from the controls (**Figure 7H**). Overall, these tracking analyses show that in developing lateral-line hair cells, the kinesin motor Kif1aa is not essential for directional motion of ribbons and precursors. In contrast, an unperturbed microtubule network is essential for this directed motion.

Ribbon precursors fuse on microtubules

Our analyses demonstrate that movement of ribbon precursors along microtubules is important for synapse formation. But in addition to movement, during development it has been proposed that these small precursors come together or fuse to form larger, more mature ribbons (Michanski et al., 2019). This is consistent with our work, where we see a reduction in ribbon and precursor number alongside development (**Figure 1E**). Further we see an increase in ribbon and precursor number when microtubules are destabilized (**Figure 4**), indicating an intact microtubule network may also be important for ribbon fusion.

Consistent with this idea, in our timelapses, we observed that ribbons and precursors undergo fusion on microtubules to form larger ribbons. These fusion events occurred between smaller precursors at the cell apex as well as between larger precursors near the cell base (examples: **Figure 8A-B**, **Figure 8**-S1A-B, Movies S8-S10). We classified an event as a fusion once the ribbons could not be resolved separately and stayed together for the length of the remaining timelapse (or at least 5 min). These events usually involved ribbon precursors on two separate microtubule filaments coming together during fusion, but fusion events could also occur on the same filament. Although the fusion events were infrequent, within our time windows (30-70 mins), we quantified them and counted an average of 1.7 fusions and a maximum of 5 fusions events per neuromast in developing lateral-line hair cells (n = 27 control neuromasts). Based on the close association with microtubules during these events we tested whether an intact microtubule network was required for fusion events. We found that after treatment with 500 nM

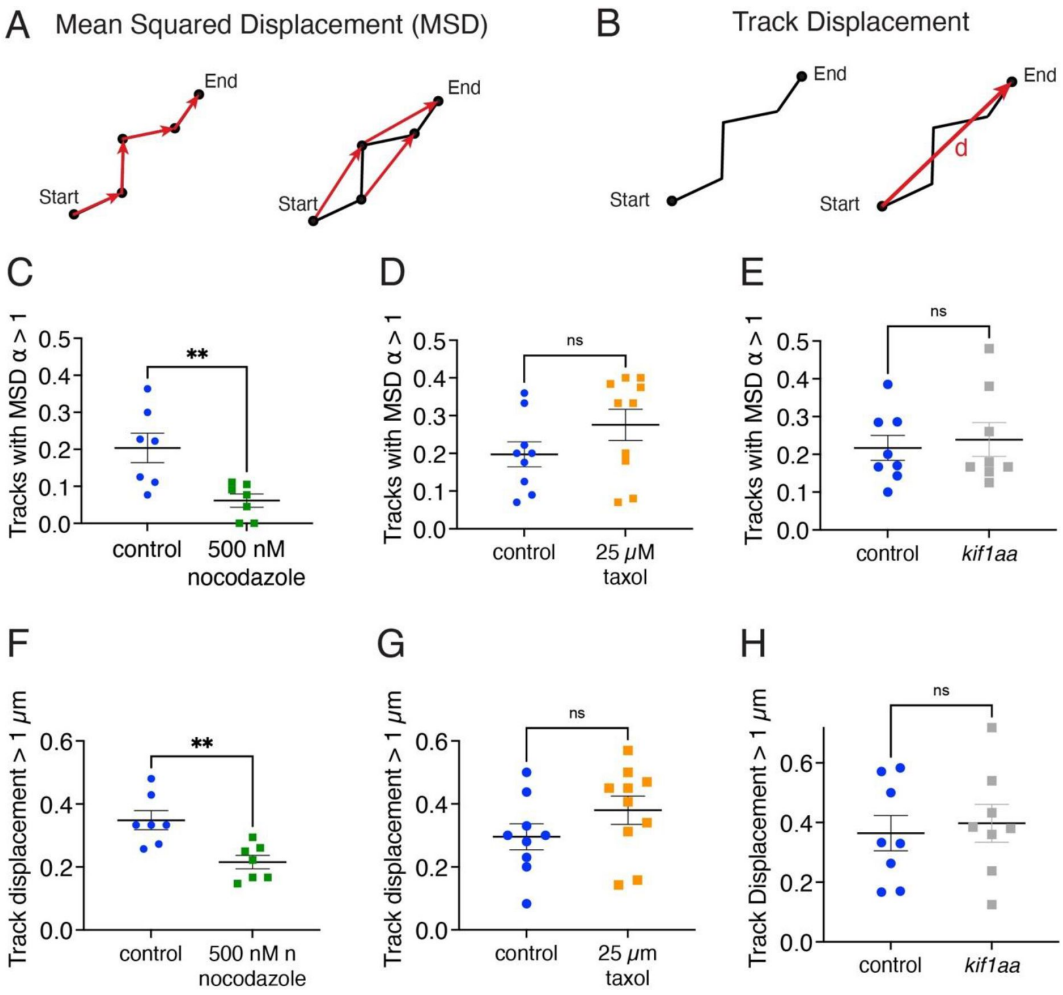

Figure 7

Ribbon precursors require intact microtubules, but not Kif1aa for directional motion **A)** Mean squared displacement (MSD) vs time was used to quantify the proportion of ribbon and precursor tracks with a velocity have α > 1, a behavior indicative of directionally moving tracks. **B)** To further quantify directional motion, the proportion of tracks with large displacements (>1 μm) was quantified. Track displacement was measured as the distance between the start and end point of the track. **C)** Hair cells treated with 500 mM nocodazole have fewer directional tracks (α > 1) as compared to controls (p = 0.007). **D)** In hair cells treated with 25 μM taxol there are not significantly fewer directional tracks (α > 1) compared to controls (p = 0.24). **E)** In hair cells lacking Kif1aa, there are not significantly fewer directional tracks (α > 1) compared to controls (p =0.70). **F)** Hairs cells treated with 500 mM nocodazole have fewer ribbons with track displacements > 1 μm as compared to control (p = 0.004). **G)** There is no change in ribbon displacement> 1 μm in hair cells treated with 25 μM taxol (p = 0.17). **H)** There is no change in ribbon displacement >1 μm in hair cells lacking Kif1aa (p = 0.71). N = 7 neuromasts for DMSO control and nocodazole for **C** and **F**; n = 9 and 10 neuromasts for DMSO control and taxol for **D** and **G**; n = 8 neuromasts for control and *kif1aa* for **E** and **H**. An unpaired t-test was used in **C-H**.

nocodazole for 30 minutes, there were fewer fusions events (mean 0.4, maximum 2 fusions per neuromast, n = 10 neuromasts). In contrast, the frequency of fusion events remained unchanged upon treatment with 25 μM taxol for 30 minutes.

In our tracking analysis we observed that Kif1aa was not required for directional motion of ribbon and precursors in developing hair cells (**Figure 7E,H**). But our immunohistological analyses indicated that there are more precursors and fewer complete synapses in *kif1aa* mutants. Therefore, we examined whether Kif1aa was important for fusion events. For this analysis, we quantified fusion events in *kif1aa* F0 crispants. We observed that similar to nocodazole treatment, there were significantly fewer fusions events in *kif1aa* F0 crispants (mean 0.6, maximum 2 fusions per neuromast, n = 9 neuromasts). This reduction in fusion events may ultimately account for the excess of precursors and fewer complete synapses observed in *kif1aa* mutants (**Figure 5**). Together our results indicate that during development, ribbon precursors can fuse when associated with microtubules and an unperturbed microtubule network, along with Kif1aa is needed for these fusion events.

Discussion

Our work in zebrafish applied high resolution imaging approaches to investigate how ribbons are assembled and mobilized in developing hair cells. Our study demonstrates that hair cells have microtubule networks that are polarized with the plus-end pointed to the cell base. Live- imaging approaches highlight that during development, ribbons and precursors show directed motion and fusion along microtubules, and that an intact microtubule network is important for ribbon-synapse formation.

Comparison of ribbon synapse formation in zebrafish and mice

Compared to zebrafish hair cells (12-18 hrs), synapse formation and refinement occurs over a relatively long time-window in mouse IHCs (E18-P14). In mice, much of the initial synaptogenesis occurs embryonically, while synapse refinement and pruning occur later, during first postnatal week. Due to the rapid time course of ribbon-synapse development in zebrafish, our experiments likely encompass ribbon precursors movement during synaptogenesis and synapse refinement. Our companion paper on mouse IHCs focused primarily on ribbon mobility during the dramatic pruning of synapses that occurs during early postnatal development (Vorn et al.). Unfortunately, it was not possible to study earlier events in mouse IHCs, as equivalent experiments were not possible embryonically. Live imaging at postnatal stages in mice indicates that during synapse pruning in IHCs, ribbons may detach from the membrane and undergo local trafficking and fuse to nearby presynaptic AZs. Together our studies in zebrafish and mouse hair cells illuminate several common features that characterize ribbon and microtubule dynamics during ribbon-synapse formation.

First, immunostaining in both zebrafish and mice revealed an extensive network of microtubules within hair cells. In both species, the majority of microtubules were stabilized by tubulin acetylation (**Figure 2**-S1). Our *in vivo* imaging of EB3-GFP in zebrafish hair cells revealed that microtubules are very dynamic, and the plus ends of microtubules grow towards the cell base, towards the presynaptic AZ (**Figure 2**). This data is consistent with data in mouse IHCs demonstrated via immunostaining that the minus end marker of microtubules, CAMSAP2, localizes to the IHC apex (Vorn et. al.). Overall, these studies demonstrate that microtubule networks in developing hair cells are polarized with the plus-end pointed to the cell base.

Second, live imaging in zebrafish and mouse hair cells revealed that ribbons associate with and move along microtubules. Tracking and quantification of ribbon movement via MSD analysis revealed that in both zebrafish and mouse hair cells many ribbons show motion indicative of

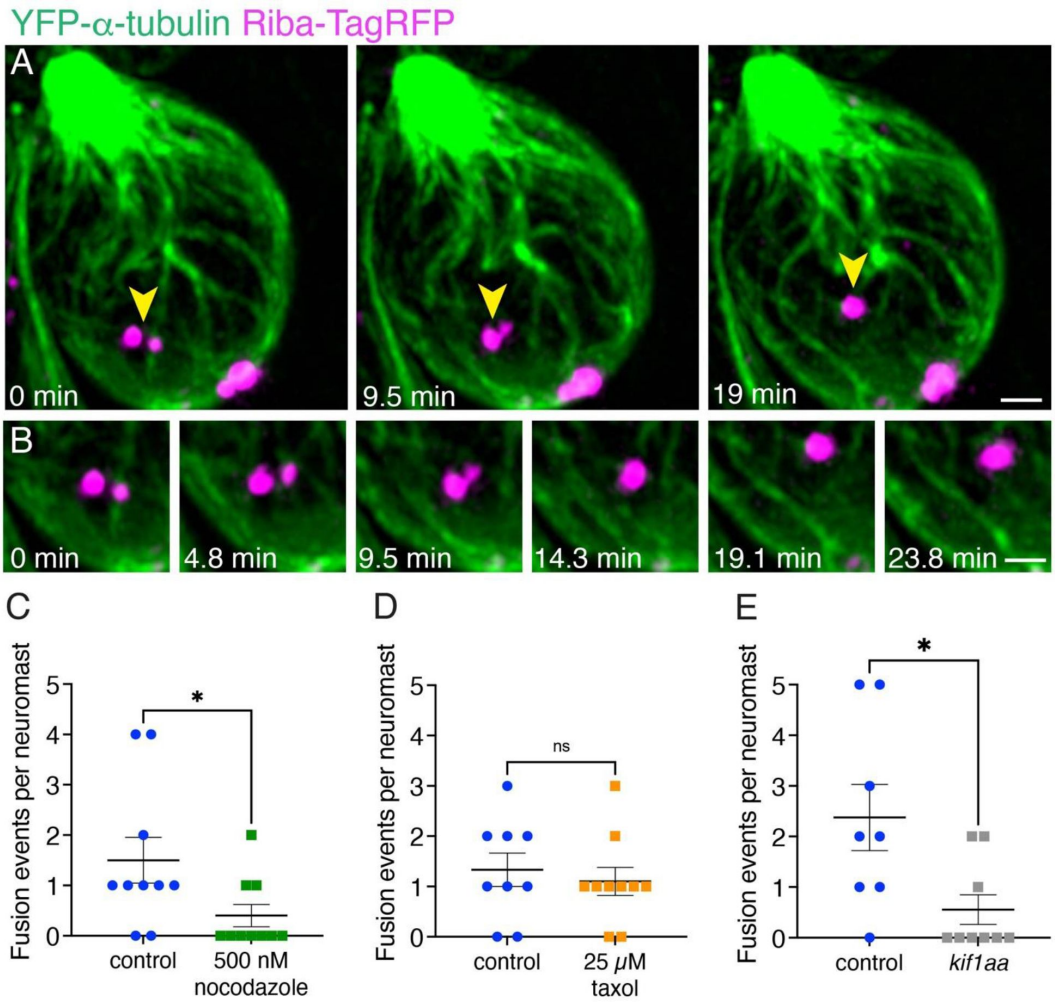

Figure 8

Ribbon precursors and Kif1aa are required for fusion events that occur on microtubules **A)** An example of two ribbon precursors undergoing fusion on microtubules to form a larger ribbon (yellow arrowheads). **B)** A zoomed in montage of the example from **A** is shown where the association of each precursor with microtubules can be seen during the process of fusion (also see Movie S8). **C-D)** Destabilizing the microtubules with nocodazole treatment reduces the number of fusion events observed in timelapses (p = 0.035). Taxol treatment has no effect (p = 0.60). **E)** Loss of Kif1aa significantly reduces the number of fusion events observed in timelapses compared to control (p = 0.018). N = 10 neuromasts for DMSO control and nocodazole for **C**; n = 9 and 10 neuromasts for DMSO control and taxol for **D**; n = 8 and 9 neuromasts for control and *kif1aa* for **E**. An unpaired t-test was used for comparisons in **D** and **E**, and a Mann-Whitney t- test was used in **C**. Scale bars in **A** and **B** = 1 μm.

confinement (**Figure 3**, $\alpha < 1$). In addition, a subset of ribbon tracks show evidence or directed motion (**Figure 3**, $\alpha > 1$). In both species, after using nocodazole to destabilize microtubules, there was a dramatic reduction in instances of directed motion (**Figure 7**). In addition to ribbon movement, ribbon fusion was observed in hair cells of mouse and zebrafish (**Figure 8**). Interestingly in mice many fusion events were balanced out by divisions, or ribbons undergoing separation. In contrast, ribbon divisions were not prevalent in zebrafish hair cells. A lack of ribbon divisions could be due to the rapid speed of development in zebrafish hair cells, where divisions are too transient in nature to be confirmed. Alternatively, divisions may occur primarily late in synapse development and these events were overall less abundant in our zebrafish datasets. Importantly, in both mouse and zebrafish, ribbon fusion was diminished after microtubule destabilization. Together these results in mice and zebrafish demonstrate that an intact microtubule network is required for the directed motion and fusion of ribbons during development.

Third, we sought to explore the kinesin motor responsible for ribbon movement in hair cells using zebrafish and mouse models. Based on scRNAseq data and previous immunostaining evidence we focused on Kif1a (Lush et al., 2019; Michanski et al., 2019). In both mouse *Kif1a* and zebrafish *kif1aa* mutants, a common observation was an overall reduction in ribbon volume (**Figure 5**). This suggests that a conserved mechanism where both intact microtubules and Kif1aa are required for normal ribbon-synapse formation. Despite these results, future work in zebrafish and mice is needed to explore additional kinesin motors that can drive ribbon movement during synapse formation.

Fusion on microtubules as a mechanism for ribbon enlargement and maturation

Numerous studies have documented small ribbon precursors in developing photoreceptors and hair cells; later in development there are fewer, large ribbons present (Michanski et al., 2019; Regus-Leidig et al., 2009; Schmitz, 2009; Sheets et al., 2011; Sobkowicz et al., 1986, 1982). This has led to the hypothesis that ribbon precursor fusion is a mechanism to form larger, more mature ribbons (Michanski et al., 2019). Our live imaging experiments show that ribbon fusion is indeed a feature of ribbon formation (**Figure 8**, **Figure 8**-S1). Interestingly, we observed that fusion often occurs between precursors on adjacent microtubules. Fusion events can occur both apically and basally within hair cells. More apical fusion events are likely a way to increase ribbon size early in development. More basal fusion events could represent the synapse reduction and refinement that occurs later in synapse development. Whether these later, basal fusion events occur after postsynaptic elements are present is unclear and awaits additional studies. Importantly we found that the number of fusion events is decreased when microtubule networks were disrupted or when Kif1aa was absent (**Figure 8**). Together these results confirm the hypothesis that ribbons fuse during development. In addition, our work demonstrates that microtubules and Kif1aa are necessary for fusion and may help facilitate this process.

Ribbons are aggregates of proteins that share many features with biomolecular condensates that form through liquid–liquid phase separation (LLPS) (Wang et al., 2021). Biomolecular condensates are nano- to micro-meter scale compartments that function to concentrate proteins and nucleic acids. Some examples of biomolecular condensates include tight-junctions, postsynaptic densities, ribonucleoprotein (RNP) granules, and stress granules (Wang et al., 2021; Wiegand and Hyman, 2020). These condensates are highly mobile and dynamic and constituent molecules diffuse readily and exchange with the surrounding environment. Biomolecular condensates often undergo fusion to form larger ones, and then shrink into a spherical shape (Wiegand and Hyman, 2020). FRAP analyses of Ribeye-GFP labeled ribbons in hair cells have confirmed that tagged Ribeye has a fast recovery phase within ribbons, verifying that Ribeye is highly mobile and dynamic within ribbons (Graydon et al., 2017). Further, these FRAP studies revealed that Ribeye molecules can exchange with the surrounding environment. Our present

studies confirmed that ribbon precursors undergo fusion to form larger spherical ribbons (**Figure 8A,B**). Together these studies point towards the idea that precursors and ribbons are indeed biomolecular condensates. Ribeye also contains sequences predicted to be intrinsically disordered, another feature of molecules that can mediate condensate formation. Interestingly, several biomolecular condensates such as RNP transport granules are known to be transported along the microtubules (Knowles at al., 1996), similar to our observations of ribbon precursor transport.

In our current study we also found that microtubules are needed for fusion (**Figure 8C**). In other cellular contexts, the energy released by dynamic microtubules via growth and shrinkage can be used for force generation in a wide range of processes (Vleugel et al., 2016). Interestingly work on stress granules condensates, found a connection between dynamic microtubules and stress granule formation. This work demonstrated that microtubule growth and shrinkage promoted the fusion of small cytoplasmic granules into larger ones (Chernov et al., 2009). In addition, this study also demonstrated that stress granules slide along microtubules, and that this movement may act in conjunction with pushing or pulling to promote fusion (Chernov et al., 2009). Similar interactions could occur between ribbons and microtubules during development to promote fusion. Disruption of microtubules would then destabilize the formation of larger ribbons. This is consistent with our results, where we observed in more precursors and fewer mature ribbon synapses after nocodazole treatment (**Figure 4F,G**).

We also observed that fusion was disrupted in *kif1aa* mutants, despite finding that directed transport of precursors and ribbons remained unchanged in *kif1aa* mutants (**Figure 7**,**8**). A recent study on RNP condensates examined kinesin motors and adaptors in the context of microtubules (Cochard et al., 2023). This work found that the precise combination of motor proteins or adaptors can impact where condensates form. Some combinations enabled the formation and transport of condensates along microtubules. But other combinations restricted condensate formation to microtubule terminals where motor proteins are predicted to form a scaffold. Our work indicates that while more than one kinesin motor protein is capable of transporting ribbons precursors, it is predominantly Kif1aa that mediates fusion along microtubules. This could explain why precursor fusion, but not transport is impacted in *kif1aa* mutants (**Figure 7**,**8**). This scenario could also explain the extra precursors and fewer complete synapses that form in *kif1aa* mutants over time (**Figure 5**).

Kinesin motors and adaptors for ribbon transport on microtubules

Our immunohistochemistry analyses show clear synaptic defects in *kif1aa* mutants after the bulk of synapse formation has occurred (fewer synapses, more precursors, **Figure 5**). Despite these defects, we were unable to demonstrate that loss of Kif1aa impacts the movement of precursors along microtubules (**Figure 7**). These results suggests that another kinesin motor may function to transport precursors and ribbons. Pulldown assay have shown an interaction of Kif3a with Ribeye (Uthaiah and Hudspeth, 2010). While *kif1aa* mRNA is the most abundant kinesin motor protein transcript detected in lateral-line hair cells, *kif3a* mRNA is also present.

Kif3a mRNA is present at lower levels and is expressed more broadly in lateral-line hair cells, supporting cells and afferent neurons (Sur et al., 2023). Therefore, it is possible that both Kif1aa and Kif3a are competent to transport developing ribbons. Future work exploring the role of Kif3a separately or in combination with Kif1aa will illuminate the role these motors play in hair- cell synapse assembly.

Regardless of the anterograde kinesin motor(s) that transports precursors to the cell base, we also observed that precursors can also move in the retrograde direction, towards the cell apex (**Figure 3C** bottom panels and **Figure 3**-S1B). In fact, out of the tracks with directional motion, we found that 21.2 % of precursor tracks moved apically. This could be due to the fact that a subpopulation of microtubules shows plus-end mediated growth apically (22.8 %).

Alternatively, it is possible that retrograde motors may also transport ribbon precursors. For example, this could be accomplished using minus-end directed motors, such as cytoplasmic dynein heavy chain, or kinesins in the kinesin-14 family (Sweeney and Holzbaur, 2018; Yamada et al., 2017). In the future it will be important to explore the role of these additional motor proteins in the context of ribbon and precursor mobility.

It is clear from our work that ribbons and precursors show directed motion indicative of motor-mediated transport (**Figure 3** and **7**). An important part of transport is adaptor proteins that selectively link cargos to specific motor proteins (Fu and Holzbaur, 2014). In neurons, cargos leave the Golgi apparatus and are packed into specialized transport vesicles, along with adaptor scaffolds (Farías et al., 2012; Sampo et al., 2003). Work in neurons has shown that the Kif1a motor transports Rab3-positive synaptic vesicle precursors (Okada et al., 1995). This transport is thought to rely on DENN (differentially expressed in normal and neoplastic cells)/MADD (MAP kinase activating death domain) which links synaptic vesicle precursors to Kif1a (Hummel and Hoogenraad, 2021; Niwa et al., 2008). Interesting, like mature ribbons, ribbon precursors are decorated with synaptic vesicles (Michanski et al., 2019). Thus, is it possible that these synaptic vesicles may contain adaptor proteins that couple the ribbon to a kinesin motor to enable transport. In the future it will be important to identify this adaptor protein, and to understand what other molecules are co-transported with Ribeye during ribbon formation.

Ribbon formation in the absence of microtubules

Our work indicates that over short time scales (30-70 mins), when microtubules are destabilized via nocodazole treatment, fewer ribbons and precursors show directed motion indicative of active transport (**Figure 7**). In addition, when hair cells are treated with nocodazole for the entire duration of development (16 hrs) fewer synapses form (**Figure 4**). But in both of these treatment paradigms, some ribbons still show directed motion, and some synapses still form, even when microtubules are disrupted. If tracks of microtubules are required for developing precursors and ribbons mobility during development what underlies this residual movement and synapse formation?

One possibility is that not all microtubules are disrupted after nocodazole treatment. Nocodazole treatment can be cytotoxic, especially at doses high enough to eliminate all microtubules (~40 μM) (Laisne et al., 2021). The nocodazole doses we tested were not cytotoxic (100-500 nM), although higher doses did result in death of hair cells. At these lower doses it was difficult to eliminate all microtubules, especially those located more apically, which appear to be extremely stable (example, **Figure 2**-S1). It is possible that the residual ribbon mobility observed during nocodazole treatment occurs along these remaining microtubules.

Alternatively, it is possible that other filaments such as actin or intermediate filaments may also play a role or aid in ribbon mobility. Work in mouse IHC has shown that actin filaments are required to regulate and organize synaptic vesicles at mature ribbon synapses (Guillet et al., 2016). In addition, in mice, the actin-based motor protein Myosin6 has been shown to localize to ribbons and loss of Myosin6 impacts ribbon-synapse number and function (Roux et al., 2009). In addition, it is possible that ribbons and precursors may also move throughout the cell via diffusion and localize to the active zone via a ‘capture’ mechanism through an adapter protein. Although we primarily see ribbons and precursors attached to microtubules, when these filaments are destabilized using nocodazole, movement could still occur via diffusion.

Once the ribbons diffuse towards the base, other presynaptic molecules, such as Bassoon, could act to anchor ribbons at the active zone (Jing et al., 2013). Any of these scenarios could explain how ribbons move and how synapses form when microtubules are destabilized. In all likelihood, transport along microtubules, other cytoskeletal filaments, and diffusive movement are all required to ensure that ribbon synapses form properly. Additional pharmacology and imaging experiments are needed to delineate between these possibilities.

Does spontaneous activity shape ribbon transport or fusion?

In previous work we demonstrated that spontaneous calcium activity impacts ribbon formation in zebrafish hair cells (Sheets et al., 2012; Wong et al., 2019). Spontaneous activity is well documented in developing sensory systems [reviewed in: (Leighton and Lohmann, 2016)]. In the inner ear of mammals, spontaneous activity in sensory hair cells is thought to act during development to establish neuronal connections within the inner ear, and to act downstream in the brain to shape tonotopic maps (Ceriani et al., 2019; Tritsch et al., 2007). In our previous work in lateral-line hair cells, we found that spontaneous rises in presynaptic-calcium loads calcium into synaptic mitochondria. Calcium loading into the mitochondria regulates the mount of NAD^+ to NAD(H) in the developing hair cell. Blocking either presynaptic or mitochondria calcium during development results in higher levels of NAD^+, the formation of larger ribbons, fewer synapses, and the retention of small ribbon precursors in hair cells (Sheets et al., 2012; Wong et al., 2019). What aspect of ribbon formation is impacted by spontaneous activity remains unclear.

Work in yeast has shown that calcium is important for microtubule stability (Adamíková et al., 2004; Façanha et al., 2002). In addition, work in dendritic spines has shown that synaptic calcium responses promote microtubule entry into active spines (Merriam et al., 2013).

Therefore, it is possible that spontaneous calcium activity may act to stabilize microtubules or facilitate movement to the presynaptic AZ to facilitate ribbon transport. In addition to altering the microtubule network, spontaneous activity could also impact ribbon fusion. Protein condensate formation and fusion is influenced by many aspects of the cellular environment, including temperature, pH, osmolarity and ion concentration (Wang et al., 2022). Elevated calcium can promote the fusion of chromogranin proteins that undergo LLPS in the Golgi lumen (Gerdes et al., 1989; Yoo, 1995). Therefore, it is possible that elevated calcium during a spontaneous calcium event could promote ribbon or precursor fusion. In addition to the cellular environment, posttranslational modifications to the proteins within the condensate can impact formation and LLPS. Such modifications include: phosphorylation, acetylation, SUMOylation, ubiquitination, methylation, and ADP-ribosylation (Luo et al., 2021). These modifications can alter protein-protein interactions by changing the charge, structure, or hydrophobicity. Our previous work implicated that NAD^+ or NAD(H) via a NAD^+/NADH binding domain on Ribeye, could impact ribbon formation (Wong et al., 2019). It is possible that in addition to calcium, NAD^+/NADH levels in the cell could modify Ribeye to facilitate condensate formation or fusion. In the future it will be important to use the live imaging approaches outlined here to understand how spontaneous presynaptic- and mitochondrial-calcium influx impact the movement and fusion of ribbon precursors.

Overall, our live imaging studies demonstrate that microtubule networks are critical for ribbon and precursor mobility, and fusion in developing zebrafish hair cells. But ribbon synapses contain many molecules, and synapse formation requires many successive steps. In the future it will be important to develop approaches to tag and label other presynaptic ($Ca_V1.3$ channels, Bassoon, Piccolino) and postsynaptic proteins (PSD95, GluR2) that make up ribbon synapses.

For this future work, zebrafish is an ideal model system for creating these new genetic tools and for live imaging studies. By imaging ribbons, along with these other tagged synaptic components, we will gain a more comprehensive picture of ribbon-synapse formation.

Understanding how ribbon synapses form is essential to determine how to reform synapses when they are disrupted in auditory and visual disorders.

Methods

Zebrafish animals

Zebrafish (*Danio rerio*) were bred and cared for at the National Institutes of Health (NIH) under animal study protocol #1362-13. Zebrafish larvae raised at 28°C in E3 embryo medium (5 mM NaCl, 0.17 mM KCl, 0.33 mM $CaCl_2$, and 0.33 mM $MgSO_4$, buffered in HEPES, pH 7.2). All experiments were performed on larvae aged 2-3 days post fertilization (dpf). Larvae were chosen at random at an age where sex determination is not possible. The previously described mutant and transgenic lines were used in this study: *Tg(myo6b:ctbp2a-TagRFP)*^{idc11Tg} referred to as *myo6b:riba-TagRFP; Tg(myo6b:YFP-Hsa.TUBA)*^{idc16Tg} referred to as *myo6b:YFP-tubulin* (Ohta et al., 2020; Wong et al., 2019).

Zebrafish transgenic and CRISPR-Cas9 mutant generation

To create *myo6b:EB3-GFP* transgenic fish, plasmid construction was based on the tol2/gateway zebrafish kit (Kwan et al., 2007). The p5E *pmyo6b* entry clone (Trapani et al., 2009) was used to drive expression in hair cells. A pME-*EB3-GFP* clone was kindly provided by Catherine Drerup at University of Wisconsin, Madison. pDestTol2pACryGFP was a gift from Joachim Berger & Peter Currie (Addgene plasmid # 64022). These clones were used along with the following tol2 kit gateway clone, p3E-*polyA* (#302) to create the expression construct: *myo6b:EB3-GFP*. To generate the stable transgenic fish line *myo6b:EB3-GFP*^{idc23Tg}, plasmid DNA and tol2 transposase mRNA were injected into zebrafish embryos as previously described (Kwan et al., 2007). The *myo6b:EB3-GFP*^{idc23Tg} transgenic line was selected for single copy and low expression of EB3-GFP.

A *kif1aa* germline mutant was generated in-house using CRISPR-Cas9 technology as previously described (Varshney et al., 2016). Exon 6, containing part of the Kinesin motor domain was targeted. Guides RNAs (gRNAs) targeted to *kif1aa* are as follows: 5'-ACGGATGTTCTCGCACACGT(AGG)-3', 5'-GTGCGAGAACATCCGTTGCT(AGG)-3', 5'-TGGACTCCGGGAATAAGGCT(AGG)-3', 5'-AGAATACCTAGCCTTATTCC(CGG)-3'. Founder fish were identified using fragment analysis of fluorescent PCR (fPCR) products. A founder fish containing a complex INDEL that destroys a BslI restriction site in exon 6 was selected (**Figure 5**-S1B). This INDEL disrupts the protein at amino acid 166 (**Figure 5**-S1A). Subsequent genotyping was accomplished using standard PCR and Bsl1 restriction enzyme digestion. *Kif1aa* genotyping primers used were: *kif1aa*_FWD 5'-AACACCAAGCTGACCAGTGC-3' and *kif1aa*_REV 5'-TGCGGTCCTAGGCTTACAAT-3'.

We created *kif1aa* F0 crispants for our live imaging analyses. Here we injected the following *kif1aa* gRNAs: 5'-GTGCGAGAACATCCGTTGCT(AGG)-3' and 5'- AGAATACCTAGCCTTATTCC(CGG)-3', along with Cas9 protein, as previously described (Hoshijima et al., 2019). We then grew *kif1aa* injected F0 crispants for 2 days and then used them for our live imaging analyses. Because *kif1aa* mutants have no phenotype to distinguish them from sibling controls at the ages imaged, the low throughput of our live imaging approaches made using germline mutants prohibitive. Studies have shown that F0 crispants are a fast and effective way to knockdown gene function in any genetic background (Hoshijima et al., 2019; Sheets et al., 2021). After live imaging, we genotyped all *kif1aa* F0 crispants to ensure that the gRNAs cut the target robustly using fragment analysis of fluorescent PCR products and the following primers: *kif1aa*_FWD_fPCR 5'-TGTAAAACGACGGCCAGT- AAATAGAGATTCACTTTTAATC-3' and *kif1aa*_REV_fPCR 5'- GTGTCTT-CCTAGGCTTACAATGCTTTTGG-3' (Carrington et al., 2015). Any *kif1aa* F0 crispants without robust genomic cutting were not included in analyses.

Zebrafish pharmacology

To destabilize or stabilize microtubules, larval zebrafish at 2 dpf were incubated in either nocodazole (Sigma-Aldrich, SML1665) or Paclitaxel (taxol) (Sigma-Aldrich, 5082270001). Both drugs were maintained in DMSO. For experiments these drugs were diluted in media for a final concentration of 0.1 % DMSO, 250-500 nM nocodazole and 25 µM taxol. For controls, larvae were incubated in media containing 0.1 % DMSO. For long-term incubation (16 hr), wild-type larvae were incubated in E3 media containing 250 nM nocodazole or 25 µM taxol at 54 hpf for 16 hrs (overnight). After this long-term treatment, larvae were fixed and prepared for immunohistochemistry (see below). For live, short-term incubations (for 3-4 hr incubations or ribbon tracking), transgenic larvae (*myo6b:riba-tagRFP; Tg(myo6b:YFP-alpha-tubulin*) at 48-54 hpf were embedded in 1 % low melt agarose prepared in E3 media containing 0.03 % tricaine (Sigma-Aldrich, A5040, ethyl 3-aminobenzoate methanesulfonate salt). 500 nM nocodazole, 25 µM taxol or DMSO were added to the agarose and to the E3 media used to hydrate the sample. For these short-term treatments, hair cells were imaged after 30 min of embedding.

Immunohistochemistry of zebrafish samples

Immunohistochemistry to label acetylated-tubulin, tyrosinated-tubulin, Ribeyeb (ribbons and precursors), pan-Maguk (postsynaptic densities) and Myosin7a (hair-cell bodies) was performed on whole zebrafish larvae similar to previous work. The following primary antibodies were used: rabbit anti-Myosin7a (Proteus 25-6790; 1:1000) mouse anti-pan-Maguk (IgG1) (Millipore MABN7; 1:500); mouse anti-Ribeyeb (IgG2a) ((Sheets et al., 2011); 1:10,000); mouse anti- acetylated-tubulin (IgG2b) (Sigma-Aldrich T7451; 1:5,000); mouse anti-tyrosinated-tubulin (IgG2a) (Sigma-Aldrich MAB1864-I; 1:1,000); chicken anti-GFP (to stain YFP-tubulin) (Aves labs GFP-1010; 1:1,000). The following secondary antibodies were used at 1:1,000: (ThermoFisher Scientific, A-11008; A-21143, A-21131, A-21240; A-11-039, A-21242, A-21241, A-11039). Larvae were fixed with 4 % paraformaldehyde in PBS for 4 hr at 4°C. All wash, block and antibody solutions were prepared in 0.1 % Tween in PBS (PBST). After fixation, larvae were washed 5 × 5 min in PBST. Prior to block, larvae were permeabilized with acetone. For this permeabilization larvae were first washed for 5 min with H_2O. The H_2O was removed and replaced with ice-cold acetone and placed at −20°C for 3 min, followed by a 5 min H_2O wash. The larvae were then washed for 5 × 5 min in PBST. Larvae were then blocked overnight at 4°C in blocking solution (2 % goat serum, 1 % bovine serum albumin, 2 % fish skin gelatin in PBST). Larvae were then incubated in primary antibodies in antibody solution (1 % bovine serum albumin in PBST) overnight, nutating at 4°C. The next day, the larvae were washed for 5 × 5 min in PBST to remove the primary antibodies. Secondary antibodies in antibody solution were added and larvae were incubated for 3 hrs at room temperature. After 5 × 5 min washes min in PBST to remove the secondary antibodies, larvae were rinsed in H_2O and mounted in Prolong gold (ThermoFisher Scientific P36930).

Confocal imaging and analysis of fixed zebrafish samples

After immunostaining, fixed zebrafish samples were imaged on an inverted Zeiss LSM 780 (Zen 2.3 SP1) or an upright Zeiss LSM 980 (Zen 3.4) laser-scanning confocal microscope with Airyscan using a 63x 1.4 NA oil objective lens. Z-stacks encompassing the entire neuromast were acquired every 0.17 (LSM 980) or 0.18 (LSM 780) µm with an 0.04 µm x-y pixel size and Airyscan autoprocessed in 3D.

Synaptic images from fixed samples were further processed using FIJI. Acetylated tubulin or Myosin7 label was used to manually count hair cells. Complete synapses comprised of both a Ribeyeb and Maguk puncta were also counted manually. To quantify ribbon and precursor areas, images were processed in a FIJI 'IJMacro_AIRYSCAN_simple3dSeg_noco_ribbons only.ijm' as previously described (Wong et al., 2019). Here each Airyscan z-stack was max-projected. Background was subtracted from each projection using rolling-ball subtraction. A threshold was

applied to each image, followed by segmentation to delineate individual Ribeyeb puncta. The watershed function was used to separate adjacent puncta. A list of 2D objects of individual ROIs (minimum size filter of 0.002

μm^2) was created to measure the areas of Ribeyeb puncta. Areas for all Ribeyeb puncta within each neuromast were then exported as a csv spreadsheet. For comparisons, all fixed images analyzed in FIJI were imaged and processed using the same parameters.

Confocal imaging and *in vivo* analysis of ribbon numbers in developing zebrafish hair cells

For counting ribbon numbers in developing and mature hair cells (**Figure 1**), double transgenic *myo6b:riba-TagRFP* and *myo6b:YFP-tubulin* larvae at 2 and 3 dpf were imaged. Transgenic larvae were pinned to a Sylgard-filled petri dish in E3 media containing 0.03 % tricaine and imaged on a Nikon A1R upright confocal microscope using a 60x 1 NA water objective lens.

Denoised images were acquired using NIS Elements AR 5.20.02 with an 0.425 µm z-interval, at, 16x averaging, and 0.05 µm/pixel. Z-stacks of whole neuromasts including the kinocilium were acquired in a top-down configuration using 488 and 561 nm lasers. The 488 nm laser along with a transmitted PMT (T-PMT) detector was used to capture the kinocilial heights.

For quantification of ribbon numbers at different hair-cell developmental stages (**Figure 1**), a custom-written Fiji macro “Live ribbon counter” was used to batch-process the z-stacks.

The red channel (Riba-TagRFP) of each z-stack was thresholded (threshold value = 97). Watershed was applied to the thresholded stack to separate ribbons near each other. The resulting mask from the thresholding and watershedding was applied to the original red channel. The number of ribbons was then counted using ‘3D Objects Counter’ (Threshold = 1, min size = 0, max size = 183500). The counted objects were merged with the green channel (YFP-tubulin). Each z-stack was visually inspected to determine the localization of the ribbons. Ribbons below the nucleus were classified as ‘basal’ and the rest as ‘apical’. The number of apical and basal ribbons were counted in each hair cell.

To classify the developmental stage of each hair cell (**Figure 1**), the height of the kinocilium was used. The number of z-slices between the kinocilium tip and base was determine and multiplied by the z-slice interval (0.425 µm) to get the kinocilium height. Hair cells with heights < 2.5 µm were classified as ‘Early’, hair cells with heights 2.5-10 µm were classified as ‘Intermediate’ and with heights 10-18 µm were classified as ‘Late’. Hair cells with heights > 18 µm were considered ‘Mature’.

Confocal imaging and *in vivo* tracking EB3-GFP dynamics in zebrafish

Transgenic *myo6b:EB3-GFP* larvae at 2-3 dpf were mounted in 1 % LMP agarose containing 0.03 % tricaine in a glass-bottom dish. Larvae were imaged on an inverted Zeiss LSM 780 (Zen 2.3 SP1) confocal microscope using a 63x 1.4 NA oil objective lens. For timelapses, confocal z-stacks of partial cell volumes (3.5 µm, 7 z slices at 0.5 µm z interval) with an 0.07 µm x-y pixel size were taken every 7 s for 15-30 min.

The EB3-GFP timelapses were tracked in Imaris. For spot detection, we used an estimated xy diameter of 0.534 µm with background subtraction. The detected spots were filtered by ‘Quality’ using the automatic threshold. The timelapses were visually checked to make sure the spot detection was accurate. For the tracking step, the ‘Autoregressive motion’ algorithm was used, with

a maximum linking distance of 1 µm and a maximum gap size of 3 frames. To ensure accurate track detection, short tracks were removed by filtering for the number of spots in a track (> 5) and track displacement length (> automatic threshold).

To calculate the track angles relative to the hair-cell base, we used cells that lie horizontally so we only need to consider the angles in the xy place. In Imaris, the tracks in each hair cell were selected and exported separately. Using the start and end position co-ordinates of the exported tracks, we calculated track angles in MATLAB using custom written code called, "EB3 track angle". The angle of each hair cell was measured in Imaris. The final track angle distribution plotted was obtained by measuring the difference between each track angle and the angle of the hair cell.

To create movies of EB3-GFP tracks in Movie S1, the FIJI plugin TrackMate was used (Tinevez et al., 2017). For Movie S1, the LoG detector in TrackMate was used with an estimated object diameter of 0.6 µm, a quality threshold of 8, using a median filter and sub-pixel localization. The Linear Assignment Problem (LAP) tracker was selected using frame to frame linking max distance of 1 µm, a track segment gap closing max distance of 1 µm and max frame gap of 2 µm. Tracks were colored by Track index. For viewing tracks over time, tracks were displayed as "Show tracks backwards in time" with a fade range of 5 time-points. To create color-coded temporal map of EB3-GFP tracks over a short time window (21 s, **Figure 2C-D**), the FIJI Hyperstack plugin Temporal-Color code was used with the 16 colors LUT.

Confocal imaging and *in vivo* analysis of ribbon numbers after short-term pharmacological treatments in zebrafish

For counting ribbons after 3-4 hr drug treatment, transgenic zebrafish expressing *myo6b:riba-TagRFP* and *myo6b:YFP-tubulin* at 2 dpf were examined. Transgenic larvae were mounted in 1 % low melt agarose in E3 media containing 0.03 % tricaine and one of the following: 500 nM nocodazole, 25 µM taxol or 0.1 % DMSO (Control). An inverted Zeiss LSM 780 (Zen 2.3 SP1) confocal microscope with Airyscan, along with a 63x NA 1.4 oil objective lens. Z-stacks encompassing the entire neuromast were acquired every or 0.18 µm with an 0.04 µm x-y pixel size and Airyscan autoprocessed in 3D.

To quantification of ribbon numbers before and after 3-4 hr nocodazole and taxol treatment or in *kif1aa* F0 crispants (**Figure 6**, **Figure 6**-S1), the custom-written Fiji macro "Live ribbon counter" described above was used to batch-processed the z-stacks. The red channel (Riba-TagRFP) of each z-stack was thresholded (threshold value = 28) and segmented (watershed). The resulting mask was applied to the original red channel. The number of ribbons was then counted using '3D Objects Counter' (threshold = 1, min size = 0, max size = 183500).

The counted objects were merged with the green channel (YFP-tubulin). Each z-stack was visually inspected to make sure the objects counted were within hair cells. The number of ribbons per neuromast was determined and the difference in numbers pre- and post-drug treatment was plotted.

Confocal imaging and *in vivo* tracking of ribbons

To visualize ribbon precursor movement, timelapses of double transgenic *myo6b:riba-TagRFP* and *myo6b:YFP-tubulin* larvae at 2 dpf were imaged. For pharmacological treatments, transgenic larvae were mounted in 1 % low melt agarose in E3 media containing 0.03 % tricaine and one of the following: 500 nM nocodazole, 25 µM taxol or 0.1 % DMSO (Control) in a glass- bottom dish. Double transgenic *kif1aa* crispants and uninjected controls were mounted in 1 % low melt agarose in E3 media containing 0.03 % tricaine in a glass-bottom dish. Larvae were imaged on an inverted Zeiss LSM 780 or an upright LSM 980 confocal microscope with Airyscan using a 63x 1.4 NA oil objective lens. Airyscan z-stacks of partial cell volumes (~3 µm, 16-18 z- slices using 0.18 µm z-interval and an 0.04 µm x-y pixel size) were taken on the LSM 780 every 50-100 s for 30-70 min. Faster LSM 980

Airscan z-stacks of partial cell volumes (~2-3.5 µm, 12- 20 z-slices using 0.17 µm z interval and an 0.04 µm x-y pixel size) were taken every 20 s for 15- 45 min. Airyscan timelapses were autoprocessed in 3D. In addition, we acquired a subset of LSM 780 Airscan z-stacks every 5-8 min for 30-100 min to capture fusion events more for clearly for Movies S8-10.

The longer timelapses acquired on the Zeiss LSM 780 were tracked in Imaris using spot detection with estimated xy diameters of 0.427 µm (with background subtraction). The spots were filtered based on 'Quality', with thresholds between 3-8, chosen after visual inspection of the detected spots. For tracking, the 'Autoregressive motion' algorithm was used with a maximum linking distance of 1.13 µm and a maximum gap size of 3 frames. Tracks with number of spots < 5 were not included. Using the Track displacement length filter in Imaris, the number of tracks with Track displacement length > 1 µm were counted and divided by the total number of tracks to get the fractions plotted in **Figure 7**. For the mean squared displacement (MSD) analysis, the xyzt co-ordinates were exported in 'csv' format for all tracks in a timelapse. The MSD analysis was done using the prewritten MATLAB class MSDanalyzer (Tarantino et al., 2014). MSDanalyzer calculates the mean squared displacement for each track, curve-fits the MSD vs time, and provides the value of the exponent (α). The first 25 % of the MSD vs time graph was used for curve-fitting. Tracks with the number of spots < 10 were removed to ensure accuracy of the MSD analysis.

Statistics

All data shown are mean ± standard error of the mean (SEM). All zebrafish experiments were compiled from data acquired on at least two independent days from different clutches. All replicates were biological–distinct animals and cells. Wild-type animals were selected at random for drug treatments. Datasets were excluded if there was excessive x-y-or z drift. In all datasets dot plots represent the 'n'. N represents either the number of neuromasts, hair cells, synapses or puncta as stated in the legends. For all zebrafish experiments a minimum of 3 animals and 6 neuromasts were examined. Sample sizes were selected to avoid Type 2 error. All statistical analyses were performed using Prism 10 software (GraphPad). A D'Agostino-Pearson normality test was used to test for normal distributions. To test for statistical significance between two samples, either unpaired t-tests (normally distributed data), or Wilcoxon or Mann-Whitney tests (not normally distributed data) were used. A p-value less than 0.05 was considered significant.

Contributions

KK, SH and H-TW did the immunohistochemistry, along with the imaging and analysis of fixed samples. KP and MU created the *kif1aa* mutants. KP created *kif1aa* cripants for analyses and made the *myo6b:EB3-GFP* transgenic line. SH did all the live imaging, along with the quantifications and tracking analyses. KK and SH made figures and wrote the manuscript.

Data Availability Statement

All data and code used in this paper will be available on Dyrad upon revision.

Acknowledgements

We thank Juan Angueyra and Katie Drerup for their comments on our manuscript. This work was supported by National Institute on Deafness and Other Communication Disorders (NIDCD) Intramural Research Program Grant 1ZIADC000085-01 (KK) and Project B08 of the Collaborative

Research Center 889 '*Cellular Mechanisms of Sensory Processing*' of the German Research Foundation (MU, awarded to Christian Vogl).

Supplemental Figures

Figure 1-S1

Ribbon number and apical-basal localization changes during lateral line development
A) The total number of Riba-TagRFP puncta increases from early to intermediate stages. The total number of puncta becomes significantly reduced upon maturation. **B)** The number of apically-localized Riba-TagRFP precursors is high at early and intermediate stages, and is significantly reduced compared to late and mature hair cells. **C)** The number of basally-localized Riba-TagRFP ribbons are low at early stages, and becomes significantly higher by intermediate stages. For comparisons, a Kruskal-Wallis test was used in **A-C**.

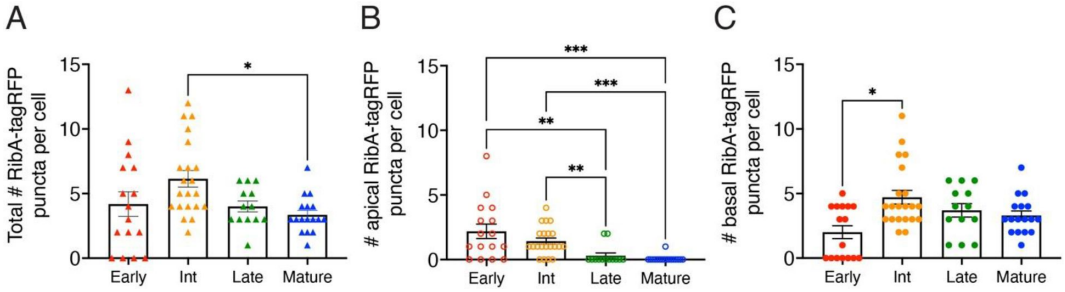

Figure 2-S1

Microtubule modifications in lateral-line hair cells **A-F)** Example immunostains of a lateral-line hair cells expressing YFP-α-tubulin at 5 dpf, labeled either with acetylated-α-tubulin (**A-C**) or tyrosinated-α-tubulin (**D-F**). Panels **A** and **D** show YFP-α-tubulin, **B** and **E** show acetylated-α-tubulin or tyrosinated-α-tubulin label respectively. Panels **C** and **F** show the merged images. HC = hair cell; SC = supporting cell; Aff = afferent process; Kino = kinocilium; Scale bar in **F** = 5 μm.

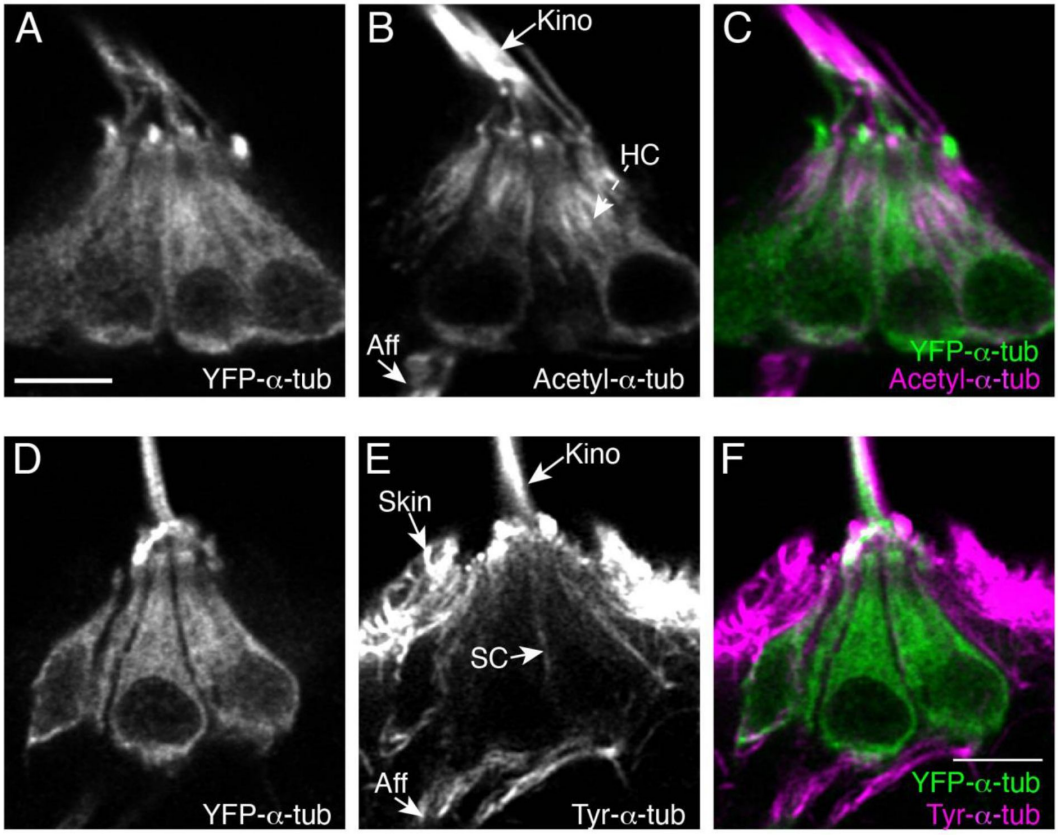

Figure 2-S2

EB3-GFP label reveals microtubule (+) ends at kinocilial tips in lateral-line hair cells **A)** Example image of EB3-GFP localization in 2 hair cells of the medial cristae within the zebrafish inner ear at 2 dpf. **B-C)** Example images of EB3-GFP localization in 4 hair cells within a lateral line neuromast at 2 dpf. In **B**, a z-projection of EB3-GFP localization in the cell bodies is shown. In **C**, a more apical projection shows the localization of EB3-GFP in the kinocilia of the same hair cells as **B**. In both zebrafish inner ear and lateral-line hair cells EB3-GFP is present in the cell bodies and at the tips of kinocilia. Scale bar in **C** = 5 µm.

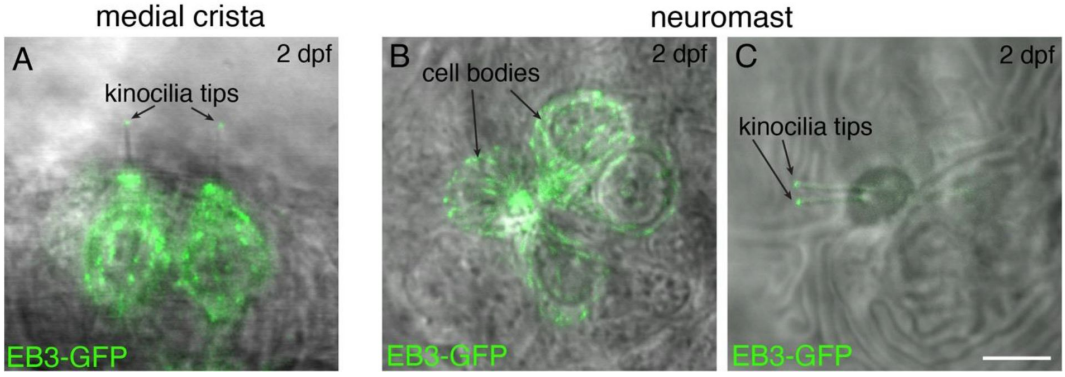

Figure 3-S1

Ribbons move directionally on microtubules and can move between microtubule filaments **A)** Example of ribbon movement on a microtubule directed towards the cells base. Ribbon precursor movement was imaged at 20 s intervals for ~40 min. Shown in **A** are frames 3, 36 and 63 (1, 12, and 21 min). **B)** Example of a ribbon movement along a microtubule towards the cell apex. Images were acquired at 50 s intervals for ~40 min. Microtubule is indicated in blue. The track of the ribbon over frames 25-46 (21 frames, 17.5 min) is shown in yellow. The track is overlaid onto the last image of the timelapse (also see Movie S5). **C)** Example of a ribbon moving along a microtubule towards the cell apex and then switching to another microtubule. Ribbon was imaged at 98 s intervals for 43 min. Shown in **C** are frames 10, 12, 14 and 16 (also see Movie S6). Scale bars in **A-C** = 1 µm.

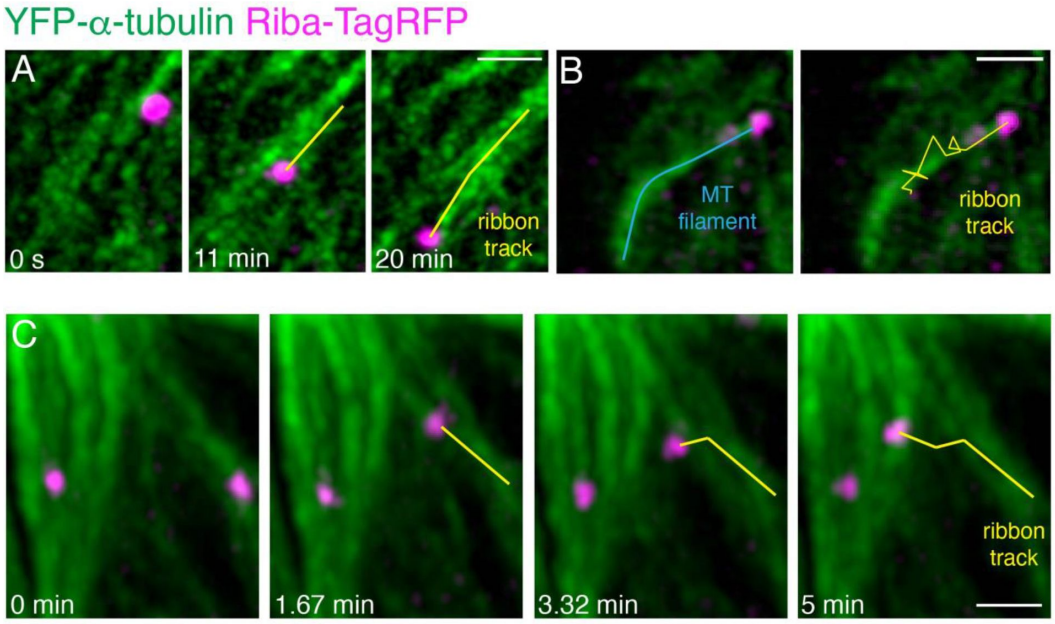

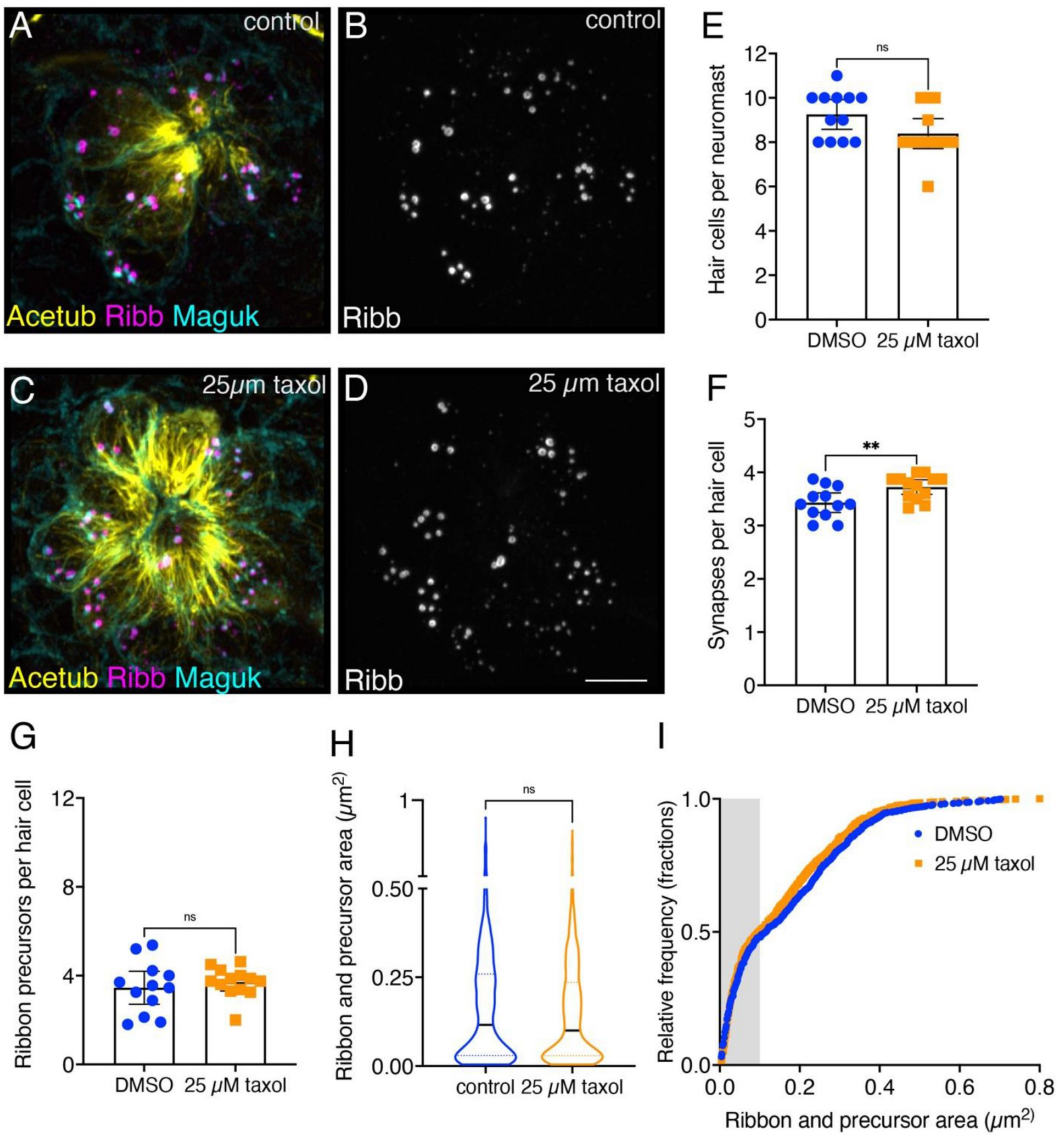

Figure 4-S1

Overnight microtubule stabilization slightly increases synapse counts **A-D)** Example immunostain of a neuromasts at 3 dpf after an overnight treatment with 25 μM taxol (**C-D**) or DMSO (**A-B**). Acetylated-α-tubulin (Acetub) labels microtubules, Ribeyeb (Ribb) labels precursors and ribbons, and Maguk labels postsynapses. **E-G**) After an overnight treatment with 25 μM taxol there are similar numbers of hair cells per neuromast (**E**, P = 0.059), more complete synapses per cell (**F**, P = 0.009), and no change in the number of ribbon precursors per cell (**G**, P = 0.398) compared to controls (n = 12 and 13 neuromasts for control and 25 μM taxol treatments). **H-I**) After an overnight treatment with 25 μM taxol the average area of Ribb puncta was not changed compared to controls (**H**, P = 0.153, n = 800 and 817 Ribb puncta for control and 25 μM taxol treatments). In **I**, the relative frequency of all the areas of Ribb puncta are plotted in taxol treatment and controls. The shaded area in **G** shows the areas (areas < 0.1 μm^2) used to quantify precursor numbers in **G**. For comparisons an unpaired t-test was used in **E-G**, and a Mann-Whitney test was used in **H**. Scale bar in **D** = 5 μm.

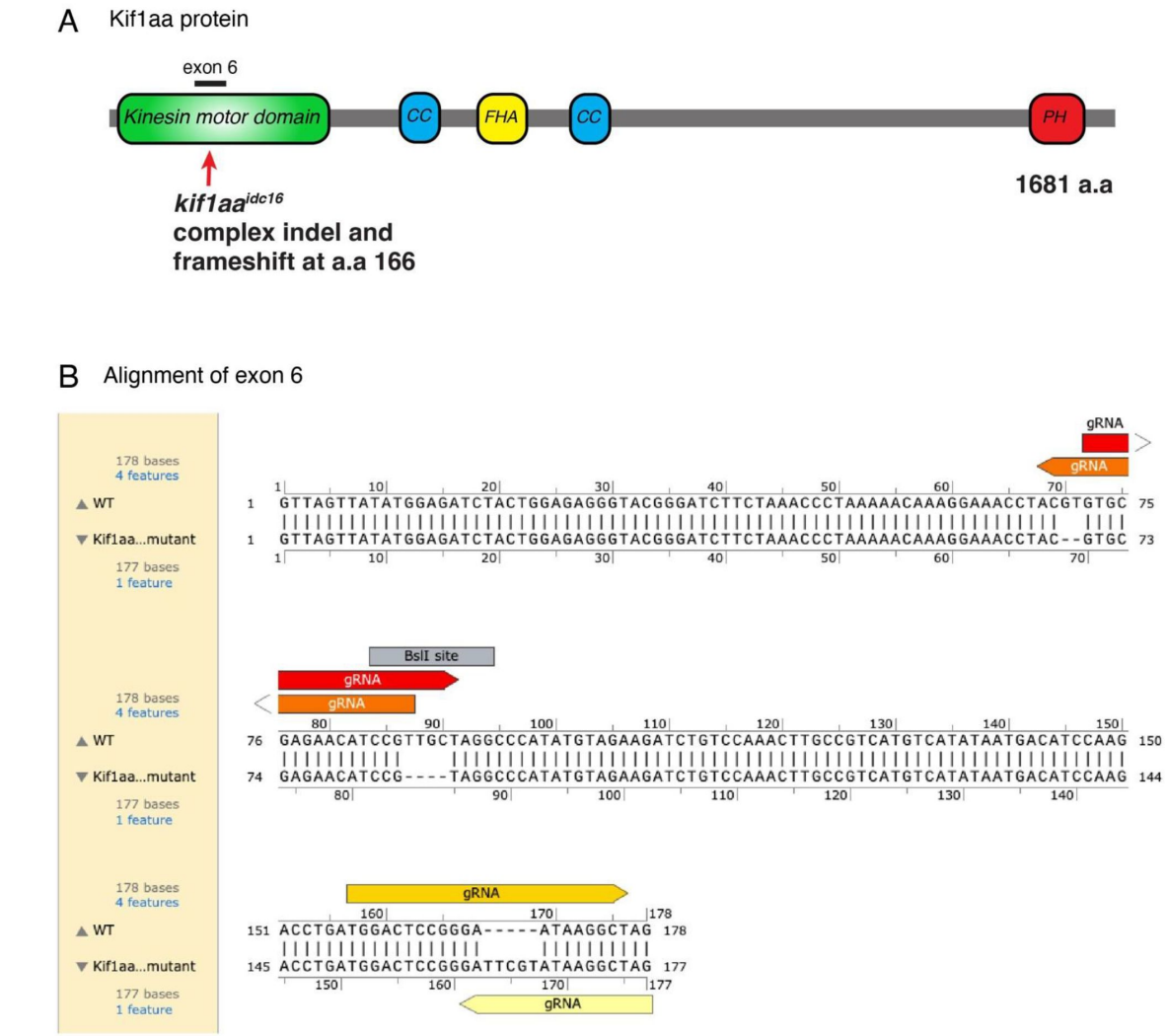

Figure 5-S1

Kif1aa protein and exon 6 lesions **A)** Overview of the Kif1aa protein and major domains (coiled coil (CC), fork-head associated (FHA), pleckstrin homology (PH)). The location of the germline *kif1aa* lesion in the Kinesin motor domain within exon 6 is indicated. **B)** The DNA sequence of exon 6 (178 bp) in wild type and *kif1aa* germline mutants. The 4 gRNAs used to make the *kif1aa* mutant are shown. 2 deletions and 1 insertion are present in *kif1aa* mutants. The BslI restriction site used for genotyping is shown. This DNA alignment was done in Snapgene.

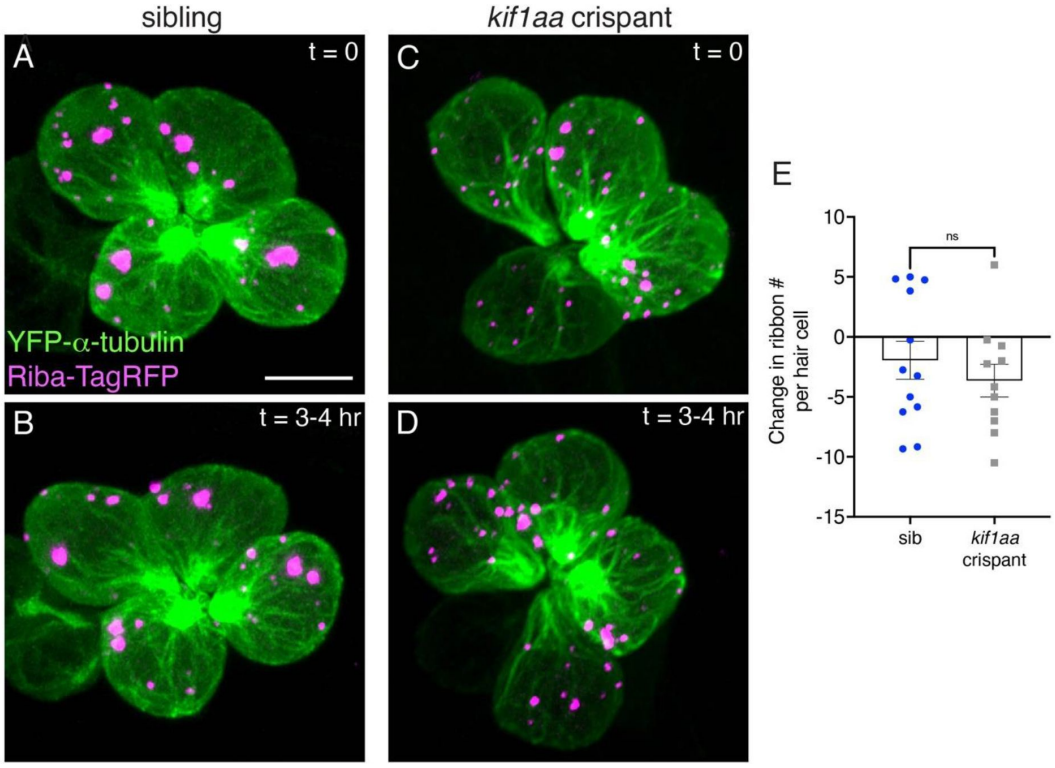

Figure 6-S1

Loss of Kif1aa does not impact ribbon numbers over 3-4 hrs **A,C)** Example images of neuromasts at 2 dpf. The microtubule network and ribbons are marked with YFP-tubulin and Riba-TagRFP respectively. Neuromasts were imaged immediately (**A**, Control; **C**, *kif1aa* F0 crispants) and after 3-4 hrs (**B**, Control; **D**, *kif1aa* F0 crispants). **E**) Quantification revealed that after 3-4 hrs the number of Riba-TagRFP puncta per hair cell was the same in control and *kif1aa* F0 crispants (n = 12 and 11 neuromasts for control and *kif1aa* F0 crispants p = 0.427). An unpaired t-test was used for comparisons in **E**. Scale bar in **A** = 5 μm.

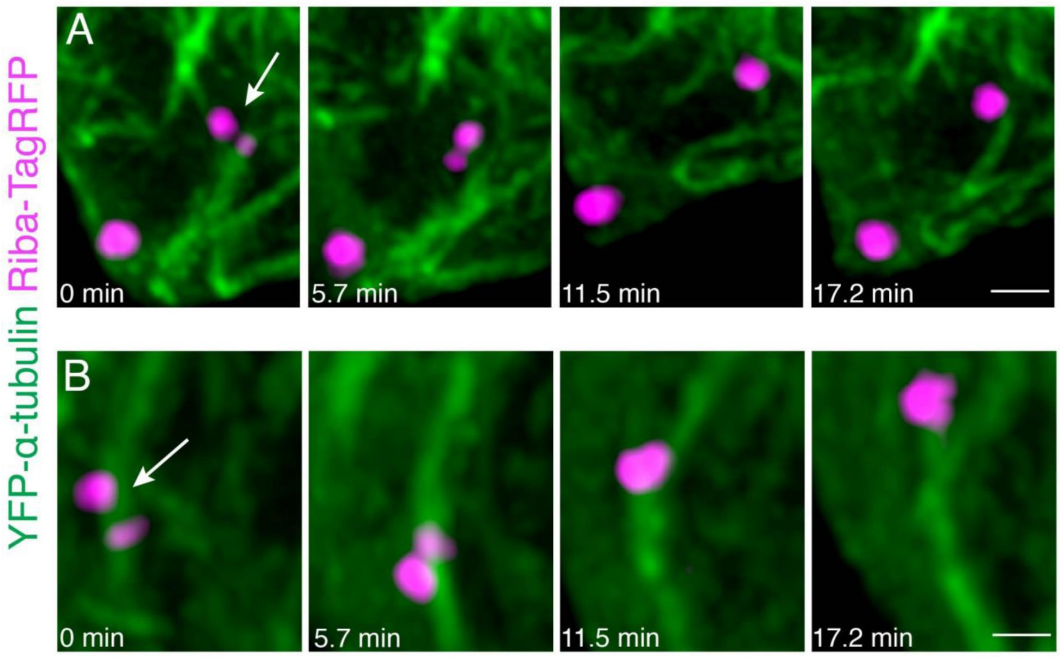

Figure 8-S1

Ribbon precursor fuse on or near microtubules **A-B)** Two examples of ribbon precursor fusion on or near microtubules. Ribbons was tracked over 13 frames that were acquired every 5.7 min. Shown in **A** are frames 3-6. Shown in **B** are frames 4-7. Arrow indicated ribbons of interest. These examples correspond to Movies S9 and S10. Scale bars in **A-B** = 1 µm.

Movie Legends

Movie S1 – EB3-GFP dynamics in developing lateral-line hair cells Timelapse of the example neuromast expressing EB3-GFP from **Figure 2**. The growing or plus- ends of microtubules can be visualized by capturing EB3-GFP dynamics. The timelapse was acquired on a LSM 780 confocal microscope every 7 s for 22 min. Maximum intensity projection of the original z-stack is shown on the left side, played at 5 frames per second. The right side shows the same movie as the left side except EB3-GFP tracks are color-coded and followed overtime using the FIJI plugin Trackmate2. Scale bar = 5 µm

Movie S2 – Tracking precursors and ribbons in 3D using Imaris Timelapse movie of a lateral-line neuromast at 2 dpf. A partial cell volume was captured at 50 s intervals for ~30 minutes with a Zeiss LSM 780 with Airyscan. Microtubules are marked with YFP-tubulin (green), ribbons and precursors are marked with Riba-TagRFP (magenta). Tracks captured in Imaris are color coded with time. This example is the same as **Figure 3A-B**. Maximum intensity projections of the original z-stack is shown, played at 5 frames per second. Scale bar = 2 µm.

Movie S3 – Tracking precursors and ribbons in 3D using Imaris Timelapse movie of a lateral-line neuromast at 2 dpf. A partial cell volume was captured at 60 s intervals for ~30 minutes with a Zeiss LSM 780 with Airyscan. Microtubules are marked with YFP-tubulin (green), ribbons and precursors are marked with Riba-TagRFP (magenta). Tracks captured in Imaris are shown in yellow. Maximum intensity projections of the original z-stack is shown, played at 5 frames per second. Scale bar = 2 µm.

Movie S4 – Directional motion to cell base and stationary precursors on microtubule Timelapse movie of a lateral-line neuromast at 2 dpf. A partial cell volume was captured at 20 s intervals for 9 minutes with a Zeiss LSM 980 with Airyscan 2. Microtubules are marked with YFP-tubulin (green), ribbons and precursors are marked with Riba-TagRFP (magenta). Maximum intensity projections of the original z-stack is shown, played at 5 frames per second. This example is the same as **Figure 3D-E**. On the left side is a timelapse of the hair cell showing a ribbon precursor moving along a microtubule towards the hair-cell base. In addition, a stationary ribbon precursor is also shown. On the right is a higher magnification view of these two ribbon precursors. The circles indicate spots identified using Trackmate, along with the track of the moving ribbon shown in yellow. Scale bar = 2 µm.

Movie S5 – Directional motion of precursor along microtubule to cell apex Timelapse movie of a lateral-line neuromast at 2 dpf. A partial cell volume was captured at 50 s intervals for 18 min with a Zeiss LSM 780 with Airyscan. Microtubules are marked with YFP- tubulin (green), ribbons and precursors are marked with Riba-TagRFP (magenta). Maximum intensity projections of the original z-stack is shown, played at 5 frames per second. On the left side is a timelapse of the hair cell showing a ribbon precursor moving along a microtubule towards the hair-cell apex. On the right is a higher magnification view of this precursor, with the tracks of the ribbon precursor during the timelapse. The circle indicate a spot identified using Trackmate, along with the track of the moving ribbon shown in yellow. This example is the same as **Figure 3**-S1B. Scale bar = 2 µm.

Movie S6 – Precursor switching between microtubules Timelapse movie of a lateral-line neuromast at 2 dpf. A partial cell volume was captured at ~100 s intervals for 40 minutes with a Zeiss LSM 970 with Airyscan. Microtubules are marked with YFP-tubulin (green), ribbons and precursors are marked with Riba-TagRFP (magenta). Maximum intensity projections of the original z-stack is shown, played at 5 frames per second. On the left side is a timelapse of the hair cell showing a ribbon precursor moving along a microtubule towards the hair cell apex; the precursor then moves to another microtubule. On the right is a higher magnification view of the

ribbon precursor during the timelapse. The precursor movement is quite fast and at this interval can be observed twice in a single z-stack during movement between microtubules at timepoints 2,4, and 15. This example is the same as **Figure 3**-S1C. Scale bar = 2 μm.

Movie S7 – Microtubule dynamics in hair cells change upon treatment with nocodazole and taxol Timelapse movies of lateral-line neuromasts at 2 dpf captured after treatment with 0.1 % DMSO (Control, left side), 25 μM taxol (Taxol, middle) or 250 nM nocodazole (Noc, right side) for 30 minutes. Microtubules are marked with YFP-tubulin (gray) and ribbons are marked with Riba-TagRFP (magenta). The timelapses were acquired in 3 um z-stacks (Zeiss LSM 780 with Airyscan) every 60 s for 30 min. Maximum intensity projections of the original z-stacks are shown here, played at 5 frames per second. The taxol-treated neuromast has less dynamic microtubules and very little cytoplasmic tubulin (depolymerized tubulin), indicating that the microtubules are more stable than the control. In the nocodazole-treated neuromast, there are less microtubules and more diffuse cytoplasmic tubulin compared to the control. Scale bar = 2 μm.

Movie S8 – Ribbon precursors attached to microtubules undergo fusion to form larger ribbons Timelapse movie of a lateral-line neuromast at 2 dpf. A partial cell volume of 3 μm was captured at 4.8 min intervals for 100 minutes with a Zeiss LSM 780 with Airyscan. Microtubules are marked with YFP-tubulin (green) and ribbons are marked with Riba-TagRFP (magenta). Maximum intensity projections of the original z-stacks are shown, played at 5 frames per second. This example is the same as **Figure 8D-E**. Two ribbon precursors associate with microtubules and fuse near the hair cell base. Scale bar = 2 μm.

Movie S9 – Ribbon precursors attached to microtubules undergo fusion to form larger ribbons Timelapse movie of a lateral-line neuromast at 2 dpf. A partial cell volume of 3 μm was captured at 5.7 min intervals for 75 minutes with a Zeiss LSM 780 with Airyscan. Microtubules are marked with YFP-tubulin (green) and ribbons are marked with Riba-TagRFP (magenta). Maximum intensity projections of the original z-stacks are shown, played at 2 frames per second. Scale bar = 2 μm.

Movie 10 – Ribbon precursors attached to microtubules undergo fusion to form larger ribbons Timelapse movie of a lateral-line neuromast at 2 dpf. A partial cell volume of 3 μm was captured at 5.7 min intervals for 75 minutes with a Zeiss LSM 780 with Airyscan. Microtubules are marked with YFP-tubulin (green) and ribbons are marked with Riba-TagRFP (magenta). Maximum intensity projections of the original z-stacks are shown, played at 2 frames per second. Scale bar = 2 μm.

References

1. Adamíková L, Straube A, Schulz I, Steinberg G (2004) **Calcium Signaling Is Involved in Dynein-dependent Microtubule Organization** *Mol Biol Cell* **15**:1969–1980 https://doi.org/10.1091/mbc.E03-09-0675

2. Ahmari SE, Buchanan J, Smith SJ (2000) **Assembly of presynaptic active zones from cytoplasmic transport packets** *Nat Neurosci* **3**:445–451 https://doi.org/10.1038/74814

3. Brandt A, Striessnig J, Moser T (2003) **CaV1.3 channels are essential for development and presynaptic activity of cochlear inner hair cells** *J Neurosci* **23**:10832–10840

4. Bury LAD, Sabo SL (2011) **Coordinated trafficking of synaptic vesicle and active zone proteins prior to synapse formation** *Neural Develop* **6** https://doi.org/10.1186/1749-8104-6-24

5. Carrington B, Varshney GK, Burgess SM, Sood R (2015) **CRISPR-STAT: an easy and reliable PCR- based method to evaluate target-specific sgRNA activity** *Nucleic Acids Res* **43** https://doi.org/10.1093/nar/gkv802

6. Ceriani F *et al.* (2019) **Coordinated calcium signalling in cochlear sensory and non-sensory cells refines afferent innervation of outer hair cells** *EMBO J* **38** https://doi.org/10.15252/embj.201899839

7. Chang B *et al.* (2006) **The nob2 mouse, a null mutation in Cacna1f: Anatomical and functional abnormalities in the outer retina and their consequences on ganglion cell visual responses** *Vis Neurosci* **23**:11–24 https://doi.org/10.1017/S095252380623102X

8. Chernov KG, Barbet A, Hamon L, Ovchinnikov LP, Curmi PA, Pastré D (2009) **Role of microtubules in stress granule assembly** *J Biol Chem* **284**:36569–36580 https://doi.org/10.1074/jbc.M109.042879

9. Cochard A, Safieddine A, Combe P, Benassy M-N, Weil D, Gueroui Z (2023) **Condensate functionalization with microtubule motors directs their nucleation in space and allows manipulating RNA localization** *EMBO J n/a:e* **114106** https://doi.org/10.15252/embj.2023114106

10. Dick O, tom Dieck S, Altrock WD, Ammermüller J, Weiler R, Garner CC, Gundelfinger ED, Brandstätter JH (2003) **The presynaptic active zone protein bassoon is essential for photoreceptor ribbon synapse formation in the retina** *Neuron* **37** https://doi.org/10.1016/s0896-6273(03)00086-2

11. Dow E, Siletti K, Hudspeth AJ (2015) **Cellular projections from sensory hair cells form polarity- specific scaffolds during synaptogenesis** *Genes Dev* **29**:1087–1094 https://doi.org/10.1101/gad.259838.115

12. Façanha ALO, Appelgren H, Tabish M, Okorokov L, Ekwall K (2002) **The endoplasmic reticulum cation P-type ATPase Cta4p is required for control of cell shape and microtubule dynamics** *J Cell Biol* **157**:1029–1039 https://doi.org/10.1083/jcb.200111012

13. Farías GG, Cuitino L, Guo X, Ren X, Jarnik M, Mattera R, Bonifacino JS (2012) **Signal-mediated, AP-1/clathrin-dependent sorting of transmembrane receptors to the somatodendritic domain of hippocampal neurons** *Neuron* **75** https://doi.org/10.1016/j.neuron.2012.07.007

14. Fejtova A *et al.* (2009) **Dynein light chain regulates axonal trafficking and synaptic levels of Bassoon** *J Cell Biol* **185**:341–355 https://doi.org/10.1083/jcb.200807155

15. Frank T *et al.* (2010) **Bassoon and the synaptic ribbon organize Ca2+ channels and vesicles to add release sites and promote refilling** *Neuron* **68**:724–738 https://doi.org/10.1016/j.neuron.2010.10.027

16. Frederick CE, Zenisek D (2023) **Ribbon synapses and retinal disease: review** *Int J Mol Sci* **24** https://doi.org/10.3390/ijms24065090

17. Freeman W (1928) **The function of the lateral line organs** *Science* **68**:205–205 https://doi.org/10.1126/science.68.1757.205

18. Fu M, Holzbaur ELF (2014) **Integrated regulation of motor-driven organelle transport by scaffolding proteins** *Trends Cell Biol* **24**:564–574 https://doi.org/10.1016/j.tcb.2014.05.002

19. Gerdes HH, Rosa P, Phillips E, Baeuerle PA, Frank R, Argos P, Huttner WB (1989) **The primary structure of human secretogranin II, a widespread tyrosine-sulfated secretory granule protein that exhibits low pH- and calcium-induced aggregation** *J Biol Chem* **264**:12009–12015 https://doi.org/10.1016/S0021-9258(18)80167-3

20. Graydon CW, Manor U, Kindt KS (2017) **In vivo ribbon mobility and turnover of Ribeye at zebrafish hair cell synapses** *Sci Rep* **7** https://doi.org/10.1038/s41598-017-07940-z

21. Guillet M, Sendin G, Bourien J, Puel J-L, Nouvian R (2016) **Actin Filaments Regulate Exocytosis at the Hair Cell Ribbon Synapse** *J Neurosci* **36**:649–654 https://doi.org/10.1523/JNEUROSCI.3379-15.2016

22. Gundelfinger ED, Reissner C, Garner CC (2016) **Role of bassoon and piccolo in assembly and molecular organization of the active zone** *Front Synaptic Neurosci* **7** https://doi.org/10.3389/fnsyn.2015.00019

23. Gupta RS (1985) **Species-specific differences in toxicity of antimitotic agents toward cultured mammalian cells2** *JNCI J Natl Cancer Inst* **74**:159–164 https://doi.org/10.1093/jnci/74.1.159

24. Hoshijima K, Jurynec MJ, Klatt Shaw D, Jacobi AM, Behlke MA, Grunwald DJ (2019) **Highly efficient crispr-cas9-based methods for generating deletion mutations and f0 embryos that lack gene function in zebrafish** *Dev Cell* **51**:645–657 https://doi.org/10.1016/j.devcel.2019.10.004

25. Hummel JJA, Hoogenraad CC (2021) **Specific KIF1A-adaptor interactions control selective cargo recognition** *J Cell Biol* **220** https://doi.org/10.1083/jcb.202105011

26. Janke C, Magiera MM (2020) **The tubulin code and its role in controlling microtubule properties and functions** *Nat Rev Mol Cell Biol* **21**:307–326 https://doi.org/10.1038/s41580-020-0214-3

27. Jean P *et al.* (2018) **The synaptic ribbon is critical for sound encoding at high rates and with temporal precision** *eLife* **7** https://doi.org/10.7554/eLife.29275

28. Jia S, Muto A, Orisme W, Henson HE, Parupalli C, Ju B, Baier H, Taylor MR (2014) **Zebrafish Cacna1fa is required for cone photoreceptor function and synaptic ribbon formation** *Hum Mol Genet* **23**:2981–2994 https://doi.org/10.1093/hmg/ddu009

29. Jing Z, Rutherford MA, Takago H, Frank T, Fejtova A, Khimich D, Moser T, Strenzke N (2013) **Disruption of the presynaptic cytomatrix protein bassoon degrades ribbon anchorage, multiquantal release, and sound encoding at the hair cell afferent synapse** *J Neurosci* **33**:4456–67 https://doi.org/10.1523/JNEUROSCI.3491-12.2013

30. Kawano D, Pinter K, Chlebowski M, Petralia RS, Wang Y-X, Nechiporuk AV, Drerup CM (2022) **NudC regulated Lis1 stability is essential for the maintenance of dynamic microtubule ends in axon terminals** *iScience* **25** https://doi.org/10.1016/j.isci.2022.105072

31. Khimich D, Nouvian R, Pujol R, Tom Dieck S, Egner A, Gundelfinger ED, Moser T (2005) **Hair cell synaptic ribbons are essential for synchronous auditory signalling** *Nature* **434**:889–894 https://doi.org/10.1038/nature03418

32. Kindt KS, Finch G, Nicolson T (2012) **Kinocilia mediate mechanosensitivity in developing zebrafish hair cells** *Dev Cell* **23**:329–341 https://doi.org/10.1016/j.devcel.2012.05.022

33. Kujawa SG, Liberman MC (2015) **Synaptopathy in the noise-exposed and aging cochlea: primary neural degeneration in acquired sensorineural hearing loss** *Hear Res* **330**:191–199 https://doi.org/10.1016/j.heares.2015.02.009

34. Kwan KM, Fujimoto E, Grabher C, Mangum BD, Hardy ME, Campbell DS, Parant JM, Yost HJ, Kanki JP, Chien C-B (2007) **The Tol2kit: a multisite gateway-based construction kit for Tol2 transposon transgenesis constructs** *Dev Dyn Off Publ Am Assoc Anat* **236**:3088–3099 https://doi.org/10.1002/dvdy.21343

35. Laisne M-C, Michallet S, Lafanechère L (2021) **Characterization of microtubule destabilizing drugs: a quantitative cell-based assay that bridges the gap between tubulin based- and cytotoxicity assays** *Cancers* **13** https://doi.org/10.3390/cancers13205226

36. Leighton AH, Lohmann C (2016) **The wiring of developing sensory circuits-from patterned spontaneous activity to synaptic plasticity mechanisms** *Front Neural Circuits* **10** https://doi.org/10.3389/fncir.2016.00071

37. Lepelletier L, de Monvel JB, Buisson J, Desdouets C, Petit C. (2013) **Auditory hair cell centrioles undergo confined brownian motion throughout the developmental migration of the kinocilium** *Biophys J* **105**:48–58 https://doi.org/10.1016/j.bpj.2013.05.009

38. Luo Y-Y, Wu J-J, Li Y-M (2021) **Regulation of liquid–liquid phase separation with focus on post- translational modifications** *Chem Commun* **57**:13275–13287 https://doi.org/10.1039/D1CC05266G

39. Lush ME *et al.* (2019) **scRNA-Seq reveals distinct stem cell populations that drive hair cell regeneration after loss of Fgf and Notch signaling** *eLife* **8** https://doi.org/10.7554/eLife.44431

40. Maas C, Torres VI, Altrock WD, Leal-Ortiz S, Wagh D, Terry-Lorenzo RT, Fejtova A, Gundelfinger ED, Ziv NE, Garner CC (2012) **Formation of Golgi-derived active zone precursor vesicles** *J Neurosci* **32**:11095–11108 https://doi.org/10.1523/JNEUROSCI.0195-12.2012

41. Magupalli VG, Schwarz K, Alpadi K, Natarajan S, Seigel GM, Schmitz F (2008) **Multiple RIBEYE-RIBEYE interactions create a dynamic scaffold for the formation of synaptic ribbons** *J Neurosci* **28**:7954–7967 https://doi.org/10.1523/JNEUROSCI.1964-08.2008

42. Mansergh F, Orton NC, Vessey JP, Lalonde MR, Stell WK, Tremblay F, Barnes S, Rancourt DE, Bech-Hansen NT (2005) **Mutation of the calcium channel gene Cacna1f disrupts calcium signaling, synaptic transmission and cellular organization in mouse retina** *Hum Mol Genet* **14**:3035–3046 https://doi.org/10.1093/hmg/ddi336

43. Maxeiner S, Luo F, Tan A, Schmitz F, Südhof TC (2016) **How to make a synaptic ribbon: RIBEYE deletion abolishes ribbons in retinal synapses and disrupts neurotransmitter release** *EMBO J* **35**:1098–1114 https://doi.org/10.15252/embj.201592701

44. Merriam EB, Millette M, Lumbard DC, Saengsawang W, Fothergill T, Hu X, Ferhat L, Dent EW (2013) **Synaptic regulation of microtubule dynamics in dendritic spines by calcium, F-actin, and drebrin** *J Neurosci* **33**:16471–16482 https://doi.org/10.1523/JNEUROSCI.0661-13.2013

45. Michanski S *et al.* (2023) **Piccolino is required for ribbon architecture at cochlear inner hair cell synapses and for hearing** *EMBO Rep n/a:e* **56702** https://doi.org/10.15252/embr.202256702

46. Michanski S *et al.* (2019) **Mapping developmental maturation of inner hair cell ribbon synapses in the apical mouse cochlea** *Proc Natl Acad Sci* **116**:6415–6424 https://doi.org/10.1073/pnas.1812029116

47. Nemzou N. RM, Bulankina AV, Khimich D, Giese A, Moser T (2006) **Synaptic organization in cochlear inner hair cells deficient for the CaV1.3 (α1D) subunit of L-type Ca2+ channels** *Neuroscience* **141**:1849–1860 https://doi.org/10.1016/j.neuroscience.2006.05.057

48. Niwa S, Tanaka Y, Hirokawa N (2008) **KIF1Bβ- and KIF1A-mediated axonal transport of presynaptic regulator Rab3 occurs in a GTP-dependent manner through DENN/MADD** *Nat Cell Biol* **10**:1269–1279 https://doi.org/10.1038/ncb1785

49. Obholzer N *et al.* (2008) **Vesicular glutamate transporter 3 is required for synaptic transmission in zebrafish hair cells** *J Neurosci* **28**:2110–2118 https://doi.org/10.1523/JNEUROSCI.5230-07.2008

50. Ohta S, Ji YR, Martin D, Wu DK (2020) **Emx2 regulates hair cell rearrangement but not positional identity within neuromasts** *eLife* https://doi.org/10.7554/eLife.60432

51. Okada Y, Yamazaki H, Sekine-Aizawa Y, Hirokawa N (1995) **The neuron-specific kinesin superfamily protein KIF1A is a unique monomeric motor for anterograde axonal transport of synaptic vesicle precursors** *Cell* **81**:769–780 https://doi.org/10.1016/0092-8674(95)90538-3

52. Oliver D, Ramachandran S, Philbrook A, Lambert CM, Nguyen KCQ, Hall DH, Francis MM (2022) **Kinesin-3 mediated axonal delivery of presynaptic neurexin stabilizes dendritic spines and postsynaptic components** *PLoS Genet* **18** https://doi.org/10.1371/journal.pgen.1010016

53. Pack-Chung E, Kurshan PT, Dickman DK, Schwarz TL (2007) **A Drosophila kinesin required for synaptic bouton formation and synaptic vesicle transport** *Nat Neurosci* **10**:980–989 https://doi.org/10.1038/nn1936

54. Regus-Leidig H, Fuchs M, Löhner M, Leist SR, Leal-Ortiz S, Chiodo VA, Hauswirth WW, Garner CC, Brandstätter JH (2014) **In vivo knockdown of Piccolino disrupts presynaptic ribbon morphology in mouse photoreceptor synapses** *Front Cell Neurosci* **8**

55. Regus-Leidig H, tom Dieck S, Specht D, Meyer L, Brandstätter JH (2009) **Early steps in the assembly of photoreceptor ribbon synapses in the mouse retina: The involvement of precursor spheres** *J Comp Neurol* **512** https://doi.org/10.1002/cne.21915

56. Roux I, Hosie S, Johnson SL, Bahloul A, Cayet N, Nouaille S, Kros CJ, Petit C, Safieddine S (2009) **Myosin VI is required for the proper maturation and function of inner hair cell ribbon synapses** *Hum Mol Genet* **18**:4615–4628 https://doi.org/10.1093/hmg/ddp429

57. Ruel J *et al.* (2008) **Impairment of SLC17A8 encoding vesicular glutamate transporter-3, VGLUT3, underlies nonsyndromic deafness DFNA25 and inner hair cell dysfunction in null mice** *Am J Hum Genet* **83** https://doi.org/10.1016/j.ajhg.2008.07.008

58. Sampo B, Kaech S, Kunz S, Banker G (2003) **Two distinct mechanisms target membrane proteins to the axonal surface** *Neuron* **37**:611–624 https://doi.org/10.1016/s0896-6273(03)00058-8

59. Schmitz F (2009) **The making of synaptic ribbons: how they are built and what they do** *Neurosci Rev J Bringing Neurobiol Neurol Psychiatry* **15**:611–624 https://doi.org/10.1177/1073858409340253

60. Schmitz F, Königstorfer A, Südhof TC (2000) **RIBEYE, a component of synaptic ribbons: a protein's journey through evolution provides insight into synaptic ribbon function** *Neuron* **28**:857–872 https://doi.org/10.1016/S0896-6273(00)00159-8

61. Schrøder JM *et al.* (2011) **EB1 and EB3 promote cilia biogenesis by several centrosome-related mechanisms** *J Cell Sci* **124**:2539–2551 https://doi.org/10.1242/jcs.085852

62. Shapira M, Zhai RG, Dresbach T, Bresler T, Torres VI, Gundelfinger ED, Ziv NE, Garner CC (2003) **Unitary assembly of presynaptic active zones from Piccolo-Bassoon transport vesicles** *Neuron* **38**:237–252 https://doi.org/10.1016/s0896-6273(03)00207-1

63. Sheets L, Holmgren M, Kindt KS (2021) **How zebrafish can drive the future of genetic-based hearing and balance research** *JARO J Assoc Res Otolaryngol* **22**:215–235 https://doi.org/10.1007/s10162-021-00798-z

64. Sheets L, Kindt KS, Nicolson T (2012) **Presynaptic CaV1.3 channels regulate synaptic ribbon size and are required for synaptic maintenance in sensory hair cells** *J Neurosci* **32**:17273–17286 https://doi.org/10.1523/JNEUROSCI.3005-12.2012

65. Sheets L, Trapani JG, Mo W, Obholzer N, Nicolson T (2011) **Ribeye is required for presynaptic Ca(V)1.3a channel localization and afferent innervation of sensory hair cells** *Dev Camb Engl* **138**:1309–1319 https://doi.org/10.1242/dev.059451

66. Sikora G, Teuerle M, Wyłomańska A, Grebenkov D (2017) **Statistical properties of the anomalous scaling exponent estimator based on time-averaged mean-square displacement** *Phys Rev E* **96** https://doi.org/10.1103/PhysRevE.96.022132

67. Sobkowicz HM, Rose JE, Scott GE, Slapnick SM (1982) **Ribbon synapses in the developing intact and cultured organ of Corti in the mouse** *J Neurosci* **2**:942–957 https://doi.org/10.1523/JNEUROSCI.02-07-00942.1982

68. Sobkowicz HM, Rose JE, Scott GL, Levenick CV (1986) **Distribution of synaptic ribbons in the developing organ of Corti** *J Neurocytol* **15**:693–714 https://doi.org/10.1007/BF01625188

69. Stepanova T, Slemmer J, Hoogenraad CC, Lansbergen G, Dortland B, Zeeuw CID, Grosveld F (2003) **Visualization of microtubule growth in cultured neurons via the use of eb3-gfp (end-binding protein 3-green fluorescent protein)** *J Neurosci* **23**:2655–2664 https://doi.org/10.1523/JNEUROSCI.23-07-02655.2003

70. Suli A, Watson GM, Rubel EW, Raible DW (2012) **Rheotaxis in larval zebrafish is mediated by lateral line mechanosensory hair cells** *PLoS ONE* **7** https://doi.org/10.1371/journal.pone.0029727

71. Sur A, Wang Y, Capar P, Margolin G, Prochaska MK, Farrell JA (2023) **Single-cell analysis of shared signatures and transcriptional diversity during zebrafish development** *Dev Cell* **58**:3028–3047 https://doi.org/10.1016/j.devcel.2023.11.001

72. Sweeney HL, Holzbaur ELF (2018) **Motor Proteins** *Cold Spring Harb Perspect Biol* **10** https://doi.org/10.1101/cshperspect.a021931

73. Tarantino N, Tinevez J-Y, Crowell EF, Boisson B, Henriques R, Mhlanga M, Agou F, Israël A, Laplantine E (2014) **TNF and IL-1 exhibit distinct ubiquitin requirements for inducing NEMO–IKK supramolecular structures** *J Cell Biol* **204**:231–245 https://doi.org/10.1083/jcb.201307172

74. Tinevez J-Y, Perry N, Schindelin J, Hoopes GM, Reynolds GD, Laplantine E, Bednarek SY, Shorte SL, Eliceiri KW (2017) **TrackMate: An open and extensible platform for single-particle tracking. Methods** *Image Processing for Biologists* **115**:80–90 https://doi.org/10.1016/j.ymeth.2016.09.016

75. Trapani JG, Obholzer N, Mo W, Brockerhoff SE, Nicolson T (2009) **Synaptojanin1 is required for temporal fidelity of synaptic transmission in hair cells** *PLOS Genet* **5** https://doi.org/10.1371/journal.pgen.1000480

76. Tritsch NX, Yi E, Gale JE, Glowatzki E, Bergles DE (2007) **The origin of spontaneous activity in the developing auditory system** *Nature* **450**:50–55 https://doi.org/10.1038/nature06233

77. Uthaiah RC, Hudspeth AJ (2010) **Molecular anatomy of the hair cell's ribbon synapse** *J Neurosci* **30**:12387–12399 https://doi.org/10.1523/JNEUROSCI.1014-10.2010

78. Varshney GK *et al.* (2016) **A high-throughput functional genomics workflow based on CRISPR/Cas9-mediated targeted mutagenesis in zebrafish** *Nat Protoc* **11**:2357–2375 https://doi.org/10.1038/nprot.2016.141

79. Vleugel M, Kok M, Dogterom M (2016) **Understanding force-generating microtubule systems through in vitro reconstitution** *Cell Adhes Migr* **10**:475–494 https://doi.org/10.1080/19336918.2016.1241923

80. Wang B, Lei Zhang, Dai T, Qin Z, Lu H, Long Zhang, Zhou F (2021) **Liquid–liquid phase separation in human health and diseases** *Signal Transduct Target Ther* **6**:1–16 https://doi.org/10.1038/s41392-021-00678-1

81. Wang Z, Lou J, Zhang H (2022) **Essence determines phenomenon: Assaying the material properties of biological condensates** *J Biol Chem* **298** https://doi.org/10.1016/j.jbc.2022.101782

82. Wiegand T, Hyman AA (2020) **Drops and fibers — how biomolecular condensates and cytoskeletal filaments influence each other** *Emerg Top Life Sci* **4**:247–261 https://doi.org/10.1042/ETLS20190174

83. Wong HC, Zhang Q, Beirl AJ, Petralia RS, Wang Y-X, Kindt K (2019) **Synaptic mitochondria regulate hair-cell synapse size and function** *eLife* **8** https://doi.org/10.7554/eLife.48914

84. Yamada M, Tanaka-Takiguchi Y, Hayashi M, Nishina M, Goshima G (2017) **Multiple kinesin-14 family members drive microtubule minus end–directed transport in plant cells** *J Cell Biol* **216**:1705–1714 https://doi.org/10.1083/jcb.201610065

85. Yoo SH (1995) **pH- and Ca2+-induced Conformational Change and Aggregation of Chromogranin B.: COMPARISON WITH CHROMOGRANIN A AND IMPLICATION IN SECRETORY VESICLE BIOGENESIS (*)** *J Biol Chem* **270**:12578–12583 https://doi.org/10.1074/jbc.270.21.12578

86. Zhang Q, Kindt KS (2022) **Using light-sheet microscopy to study spontaneous activity in the developing lateral-line system** *Front Cell Dev Biol* **10** https://doi.org/10.3389/fcell.2022.819612

87. Zieve GW, Turnbull D, Mullins JM, McIntosh JR (1980) **Production of large numbers of mitotic mammalian cells by use of the reversible microtubule inhibitor nocodazole. Nocodazole accumulated mitotic cells** *Exp Cell Res* **126**:397–405 https://doi.org/10.1016/0014-4827(80)90279-7

Editors

Reviewing Editor
Andrew King
University of Oxford, Oxford, United Kingdom

Senior Editor
Andrew King
University of Oxford, Oxford, United Kingdom

Reviewer #1 (Public Review):

Summary:

The manuscript by Hussain and collaborators aims at deciphering the microtubule-dependent ribbon formation in zebrafish hair cells. By using confocal imaging, pharmacology tools, and zebrafish mutants, the group of Katie Kindt convincingly demonstrated that ribbon, the organelle that concentrates glutamate-filled vesicles at the hair cell synapse, originates from the fusion of precursors that move along the microtubule network. This study goes hand in hand with a complementary paper (Voorn et al.) showing similar results in mouse hair cells.

Strengths:

This study clearly tracked the dynamics of the microtubules, and those of the microtubule-associated ribbons and demonstrated fusion ribbon events. In addition, the authors have identified the critical role of kinesin Kif1aa in the fusion events. The results are compelling and the images and movies are magnificent.

Weaknesses:

The lack of functional data regarding the role of Kif1aa. Although it is difficult to probe and interpret the behavior of zebrafish after nocodazole treatment, I wonder whether deletion of kif1aa in hair cells may result in a functional deficit that could be easily tested in zebrafish?

Impact:

The synaptogenesis in the auditory sensory cell remains still elusive. Here, this study indicates that the formation of the synaptic organelle is a dynamic process involving the fusion of presynaptic elements. This study will undoubtedly boost a new line of research aimed at identifying the specific molecular determinants that target ribbon precursors to the synapse and govern the fusion process.

https://doi.org/10.7554/eLife.98119.1.sa2

Reviewer #2 (Public Review):

Summary:

In this manuscript, the authors set out to resolve a long-standing mystery in the field of sensory biology - how large, presynaptic bodies called "ribbon synapses" migrate to the basolateral end of hair cells. The ribbon synapse is found in sensory hair cells and photoreceptors, and is a critical structural feature of a readily-releasable pool of glutamate that excites postsynaptic afferent neurons. For decades, we have known these structures exist, but the mechanisms that control how ribbon synapses coalesce at the bottom of hair cells are not well understood. The authors addressed this question by leveraging the highly-tractable zebrafish lateral line neuromast, which exhibits a small number of visible hair cells, easily observed in time-lapse imaging. The approach combined genetics, pharmacological manipulations, high-resolution imaging, and careful quantifications. The manuscript commences with a developmental time course of ribbon synapse development, characterizing both immature and mature ribbon bodies (defined by position in the hair cell, apical vs. basal). Next, the authors show convincing (and frankly mesmerizing) imaging data of plus end-directed microtubule trafficking toward the basal end of the hair cells, and data highlighting the directed motion of ribbon bodies. The authors then use a series of pharmacological and genetic manipulations showing the role of microtubule stability and one particular kinesin (Kif1aa) in the transport and fusion of ribbon bodies, which is presumably a prerequisite for hair cell synaptic transmission. The data suggest that microtubules and their stability are necessary for normal numbers of mature ribbons and that Kif1aa is likely required for fusion events associated with ribbon maturation. Overall, the data provide a new and interesting story on ribbon synapse dynamics.

Strengths:

(1) The manuscript offers a comprehensive Introduction and Discussion sections that will inform generalists and specialists.

(2) The use of Airyscan imaging in living samples to view and measure microtubule and ribbon dynamics in vivo represents a strength. With rigorous quantification and thoughtful analyses, the authors generate datasets often only obtained in cultured cells or more diminutive animal models (e.g., C. elegans).

(3) The number of biological replicates and the statistical analyses are strong. The combination of pharmacology and genetic manipulations also represents strong rigor.

(4) One of the most important strengths is that the manuscript and data spur on other questions - namely, do (or how do) ribbon bodies attach to Kinesin proteins? Also, and as noted in the Discussion, do hair cell activity and subsequent intracellular calcium rises facilitate ribbon transport/fusion?

Weaknesses:

(1) Neither the data or the Discussion address a direct or indirect link between Kinesins and ribbon bodies. Showing Kif1aa protein in proximity to the ribbon bodies would add strength.

(2) Neither the data or Discussion address the functional consequences of loss of Kif1aa or ribbon transport. Presumably, both manipulations would reduce afferent excitation.

(3) It is unknown whether the drug treatments or genetic manipulations are specific to hair cells, so we can't know for certain whether any phenotypic defects are secondary.

https://doi.org/10.7554/eLife.98119.1.sa1

Reviewer #3 (Public Review):

Summary:

The manuscript uses live imaging to study the role of microtubules in the movement of ribeye aggregates in neuromast hair cells in zebrafish. The main findings are that
(1) Ribeye aggregates, assumed to be ribbon precursors, move in a directed motion toward the active zone;
(2) Disruption of microtubules and kif1aa increases the number of ribeye aggregates and decreases the number of mature synapses.

The evidence for point 2 is compelling, while the evidence for point 1 is less convincing. In particular, the directed motion conclusion is dependent upon fitting of mean squared displacement that can be prone to error and variance to do stochasticity, which is not accounted for in the analysis. Only a small subset of the aggregates meet this criteria and one wonders whether the focus on this subset misses the bigger picture of what is happening with the majority of spots.

Strengths:

(1) The effects of Kif1aa removal and nocodozole on ribbon precursor number and size are convincing and novel.

(2) The live imaging of Ribeye aggregate dynamics provides interesting insight into ribbon formation. The movies showing the fusion of ribeye spots are convincing and the demonstrated effects of nocodozole and kif1aa removal on the frequency of these events is novel.

(3) The effect of nocodozole and kif1aa removal on precursor fusion is novel and interesting.

(4) The quality of the data is extremely high and the results are interesting.

Weaknesses:

(1) To image ribeye aggregates, the investigators overexpressed Ribeye-a TAGRFP under the control of a MyoVI promoter. While it is understandable why they chose to do the experiments this way, expression is not under the same transcriptional regulation as the native protein, and some caution is warranted in drawing some conclusions. For example, the reduction in the number of puncta with maturity may partially reflect the regulation of the MyoVI promoter with hair cell maturity. Similarly, it is unknown whether overexpression has the potential to saturate binding sites (for example motors), which could influence mobility.

(2) The examples of punctae colocalizing with microtubules look clear (Figures 1 F-G), but the presentation is anecdotal. It would be better and more informative, if quantified.

(3) It appears that any directed transport may be rare. Simply having an alpha >1 is not sufficient to declare movement to be directed (motor-driven transport typically has an alpha approaching 2). Due to the randomness of a random walk and errors in fits in imperfect data will yield some spread in movement driven by Brownian motion. Many of the tracks in Figure 3H look as though they might be reasonably fit by a straight line (i.e. alpha = 1).

(4) The "directed motion" shown here does not really resemble motor-driven transport observed in other systems (axonal transport, for example) even in the subset that has been picked out as examples here. While the role of microtubules and kif1aa in synapse maturation is strong, it seems likely that this role may be something non-canonical (which would be interesting).

(5) The effect of acute treatment with nocodozole on microtubules in movie 7 and Figure 6 is not obvious to me and it is clear that whatever effect it has on microtubules is incomplete.

https://doi.org/10.7554/eLife.98119.1.sa0

Author response:

> ***Public Reviews:***
>
> ***Reviewer #1 (Public Review):***
>
> *Summary:*
>
> *The manuscript by Hussain and collaborators aims at deciphering the microtubule-dependent ribbon formation in zebrafish hair cells. By using confocal imaging, pharmacology tools, and zebrafish mutants, the group of Katie Kindt convincingly demonstrated that ribbon, the organelle that concentrates glutamate-filled vesicles at the hair cell synapse, originates from the fusion of precursors that move along the microtubule network. This study goes hand in hand with a complementary paper (Voorn et al.) showing similar results in mouse hair cells.*
>
> *Strengths:*
>
> *This study clearly tracked the dynamics of the microtubules, and those of the microtubule-associated ribbons and demonstrated fusion ribbon events. In addition, the authors have identified the critical role of kinesin Kif1aa in the fusion events. The results are compelling and the images and movies are magnificent.*
>
> *Weaknesses:*
>
> *The lack of functional data regarding the role of Kif1aa. Although it is difficult to probe and interpret the behavior of zebrafish after nocodazole treatment, I wonder whether deletion of kif1aa in hair cells may result in a functional deficit that could be easily tested in zebrafish?*

We have examined functional deficits in kif1aa mutants in another paper David et al. 2024. In Submission, preprint available:

https://www.biorxiv.org/content/10.1101/2024.05.20.595037v1

In addition to playing a role in ribbon fusions, Kif1aa is also responsible for enriching glutamate-filled secretory vesicles at the presynaptic active zone. In kif1aa mutants (and crispants), vesicles are no longer localized to the hair cell base, and there is a reduction in the number of vesicles associated with presynaptic ribbons. Kif1aa mutants also have functional defects including reductions in spontaneous vesicle release and evoked postsynaptic calcium responses. Behaviorally, kif1aa mutants exhibit impaired rheotaxis, indicating defects in the lateral-line system and an inability to accurately detect water flow. Since our paper focuses on microtubule-associated ribbon movement and dynamics early in hair cell development, we have only discussed the effects of Kif1aa directly related to ribbon dynamics during this time window in this paper. In our revision, we will reference this recently submitted work.

> *Impact:*
>
> *The synaptogenesis in the auditory sensory cell remains still elusive. Here, this study indicates that the formation of the synaptic organelle is a dynamic process involving the fusion of presynaptic elements. This study will undoubtedly boost a new line of research*

> *aimed at identifying the specific molecular determinants that target ribbon precursors to the synapse and govern the fusion process.*
>
> ***Reviewer #2 (Public Review):***
>
> *Summary:*
>
> *In this manuscript, the authors set out to resolve a long-standing mystery in the field of sensory biology - how large, presynaptic bodies called "ribbon synapses" migrate to the basolateral end of hair cells. The ribbon synapse is found in sensory hair cells and photoreceptors, and is a critical structural feature of a readily-releasable pool of glutamate that excites postsynaptic afferent neurons. For decades, we have known these structures exist, but the mechanisms that control how ribbon synapses coalesce at the bottom of hair cells are not well understood. The authors addressed this question by leveraging the highly-tractable zebrafish lateral line neuromast, which exhibits a small number of visible hair cells, easily observed in time-lapse imaging. The approach combined genetics, pharmacological manipulations, high-resolution imaging, and careful quantifications. The manuscript commences with a developmental time course of ribbon synapse development, characterizing both immature and mature ribbon bodies (defined by position in the hair cell, apical vs. basal). Next, the authors show convincing (and frankly mesmerizing) imaging data of plus end-directed microtubule trafficking toward the basal end of the hair cells, and data highlighting the directed motion of ribbon bodies. The authors then use a series of pharmacological and genetic manipulations showing the role of microtubule stability and one particular kinesin (Kif1aa) in the transport and fusion of ribbon bodies, which is presumably a prerequisite for hair cell synaptic transmission. The data suggest that microtubules and their stability are necessary for normal numbers of mature ribbons and that Kif1aa is likely required for fusion events associated with ribbon maturation. Overall, the data provide a new and interesting story on ribbon synapse dynamics.*
>
> *Strengths:*
>
> *(1) The manuscript offers a comprehensive Introduction and Discussion sections that will inform generalists and specialists.*
>
> *(2) The use of Airyscan imaging in living samples to view and measure microtubule and ribbon dynamics in vivo represents a strength. With rigorous quantification and thoughtful analyses, the authors generate datasets often only obtained in cultured cells or more diminutive animal models (e.g., C. elegans).*
>
> *(3) The number of biological replicates and the statistical analyses are strong. The combination of pharmacology and genetic manipulations also represents strong rigor.*
>
> *(4) One of the most important strengths is that the manuscript and data spur on other questions - namely, do (or how do) ribbon bodies attach to Kinesin proteins? Also, and as noted in the Discussion, do hair cell activity and subsequent intracellular calcium rises facilitate ribbon transport/fusion?*

These are important strengths and we do plan to investigate adaptors and how hair cell activity impacts ribbon fusion and transport in the future!

> *Weaknesses:*
>
> *(1) Neither the data or the Discussion address a direct or indirect link between Kinesins and ribbon bodies. Showing Kif1aa protein in proximity to the ribbon bodies would add strength.*

This is a great point, and we are working to create a transgenic line with fluorescently labelled Kif1aa to directly visualize its association with ribbons. At present, we have not obtained a transgenic line, and localization of Kif1aa and ribbons in live hair cells it is beyond the scope of this paper. In our revision we will discuss this caveat.

> *(2) Neither the data or Discussion address the functional consequences of loss of Kif1aa or ribbon transport. Presumably, both manipulations would reduce afferent excitation.*

Excellent point. Please see the response above to Reviewer #1 weaknesses.

> *(3) It is unknown whether the drug treatments or genetic manipulations are specific to hair cells, so we can't know for certain whether any phenotypic defects are secondary.*

This is correct and is a caveat of our Kif1aa and drug experiments. However, to mitigate this in the pharmacological experiments, we have done the drug treatments at 3 different timescales: long-term (overnight), short-term (4 hr) and fast (30 min) treatments. The faster experiment done after 30 min drug treatment is where we observe reduced directional motion and fusions. This later experiment should not be affected by any long-term changes or developmental defects that could be caused by the drugs as hair cell development occurs over 8-12 hrs. However, we acknowledge that these treatments and genetic experiments could have secondary phenotypic defects that are not hair-cell specific. In our revision, we will discuss these issues.

> ***Reviewer #3 (Public Review):***
>
> *Summary:*
>
> *The manuscript uses live imaging to study the role of microtubules in the movement of ribeye aggregates in neuromast hair cells in zebrafish. The main findings are that*
>
> *(1) Ribeye aggregates, assumed to be ribbon precursors, move in a directed motion toward the active zone;*
>
> *(2) Disruption of microtubules and kif1aa increases the number of ribeye aggregates and decreases the number of mature synapses.*
>
> *The evidence for point 2 is compelling, while the evidence for point 1 is less convincing. In particular, the directed motion conclusion is dependent upon fitting of mean squared displacement that can be prone to error and variance to do stochasticity, which is not accounted for in the analysis. Only a small subset of the aggregates meet this criteria and one wonders whether the focus on this subset misses the bigger picture of what is happening with the majority of spots.*
>
> *Strengths:*
>
> *(1) The effects of Kif1aa removal and nocodozole on ribbon precursor number and size are convincing and novel.*
>
> *(2) The live imaging of Ribeye aggregate dynamics provides interesting insight into ribbon formation. The movies showing the fusion of ribeye spots are convincing and the demonstrated effects of nocodozole and kif1aa removal on the frequency of these events is novel.*
>
> *(3) The effect of nocodozole and kif1aa removal on precursor fusion is novel and interesting.*

> *(4) The quality of the data is extremely high and the results are interesting.*
>
> *Weaknesses:*
>
> *(1) To image ribeye aggregates, the investigators overexpressed Ribeye-a TAGRFP under the control of a MyoVI promoter. While it is understandable why they chose to do the experiments this way, expression is not under the same transcriptional regulation as the native protein, and some caution is warranted in drawing some conclusions. For example, the reduction in the number of puncta with maturity may partially reflect the regulation of the MyoVI promoter with hair cell maturity. Similarly, it is unknown whether overexpression has the potential to saturate binding sites (for example motors), which could influence mobility.*

We agree that overexpression in transgenic lines is a common issue and would have loved to do these experiments with endogenously expressed fluorescent proteins under a native promoter. However, this was not technically possible for us. We originally characterized several transgenic Ribeye lines in the past to ensure they have normal ribbon numbers and size (myo6b:ribb-mcherry, myo6b:riba-tagRFP and myo6b:riba-GFP) - in 2014. Unfortunately, we no longer have the raw data from this analysis. In our revision, we will repeat our immunolabel on myo6b:riba-tagRFP transgenic fish and examine ribbon numbers and size and show what impact (or not) exogenous Ribeye expression has on ribbon formation.

> *(2) The examples of punctae colocalizing with microtubules look clear (Figures 1 F-G), but the presentation is anecdotal. It would be better and more informative, if quantified.*

We attempted a co-localization study between microtubules and ribbons but decided not to move forward with it due to several issues:

(1) Hair cells have an extremely crowded environment, especially since the nucleus occupies the majority of the cell. All proteins are pushed together in the small space surrounding the nucleus and hence co-localization is not meaningful because the distances are so small.

(2) We also attempted to segment microtubules in these images and quantify how many ribbons were associated with microtubules, but 3D microtubule segmentation was not accurate in these hair cells due to highly varying filament intensities, and diffuse cytoplasmic tubulin signal.

Therefore, we decided that a better measure of ribbon-microtubule association would be a demonstration that individual ribbons keep their association with microtubules over time (in our time lapses), rather than a co-localization study. We see that ribbons localize to microtubules in all our timelapses, including the examples shown. We observed that if a ribbon dissociates, it is just to switch from one filament to another. We have not observed free-floating ribbons in our study.

> *(3) It appears that any directed transport may be rare. Simply having an alpha >1 is not sufficient to declare movement to be directed (motor-driven transport typically has an alpha approaching 2). Due to the randomness of a random walk and errors in fits in imperfect data will yield some spread in movement driven by Brownian motion. Many of the tracks in Figure 3H look as though they might be reasonably fit by a straight line (i.e. alpha = 1).*

As we have stated in the paper, we only see a small subset of the ribbon precursors moving directionally. The majority of the ribbons are stationary. We cannot say for sure what is happening with the stationary ribbons, but our hypothesis is that these ribbons eventually exhibit directed motion. This idea is supported by the fact that we have seen ribbons that are

stationary begin movement, and ribbons that are moving come to a stop during the acquisition of our timelapses. The ribbons that are stationary may not have enough motors attached, or they may be in a sort of 'seeding' phase where the ribeye protein could be condensing on the ribbon. We have discussed the possibility of ribbons being biomolecular condensates in our Discussion.

In our revision we will discuss why ribbon transport does not resemble typical motor-driven transport (also see response to point 4 below). We will also reexamine our MSD data in more detail as suggested by Reviewer 3 and provide distributions of alpha values in our revision.

> *(4) The "directed motion" shown here does not really resemble motor-driven transport observed in other systems (axonal transport, for example) even in the subset that has been picked out as examples here. While the role of microtubules and kif1aa in synapse maturation is strong, it seems likely that this role may be something non-canonical (which would be interesting).*

One major difference between axonal and ribbon transport is that microtubules are very stable and linear in axonal transport. Therefore, the directed motion observed is 'canonical'. In hair cells, the microtubules are extremely dynamic, especially towards the hair cell base. Within a single time frame (60-100 s), we see the network changing (moving and branching). This dynamic network adds another layer of complexity onto the motion of the ribbon, as the filament track itself is changing. Therefore, we see a lot of stalling, filament switching, and reversals of ribbon movement in our movies. However, we have demonstrated in our movies as well as using MSD analysis, that a subset of ribbons exhibit directional motion. In our revision we will discuss why directed motion in hair cells does not resemble canonical motor-driven transport in axons.

> *(5) The effect of acute treatment with nocodozole on microtubules in movie 7 and Figure 6 is not obvious to me and it is clear that whatever effect it has on microtubules is incomplete.*

When using Nocodazole, it is important to optimize the concentration of the drug such that there is minimal cytotoxicity, while still being effective. Microtubules in the apical region of hair cells are very stable and do not respond well to Nocodazole treatment at concentrations that are tolerable to hair cells. While a few stable filaments remain largely at the cell apex, there are almost no filaments at the hair cell base, which is different from the wild-type hair cells. In addition, Nocodazole-treated hair cells have more cytoplasmic YFP-tubulin signal compared to wild type. We will add additional images and quantification in our revision to illustrate these points.

https://doi.org/10.7554/eLife.98119.1.sa4